New Gene Evolution in the Bonus-TIF1-γ/TRIM33 Family Impacted the Architecture of the Vertebrate Dorsal–Ventral Patterning Network

Robert G. Wisotzkey,[†,1] Janine C. Quijano,[†,2] Michael J. Stinchfield,[2] and Stuart J. Newfeld[*,2]

[1]Department of Biological Sciences, California State University, East Bay

[2]School of Life Sciences, Arizona State University

[†]These authors contributed equally to this work.

***Corresponding author:** E-mail: newfeld@asu.edu.

Associate editor: John Logsdon

Abstract

Uncovering how a new gene acquires its function and understanding how the function of a new gene influences existing genetic networks are important topics in evolutionary biology. Here, we demonstrate nonconservation for the embryonic functions of *Drosophila* Bonus and its newest vertebrate relative TIF1-γ/TRIM33. We showed previously that TIF1-γ/TRIM33 functions as an ubiquitin ligase for the Smad4 signal transducer and antagonizes the Bone Morphogenetic Protein (BMP) signaling network underlying vertebrate dorsal–ventral axis formation. Here, we show that Bonus functions as an agonist of the Decapentaplegic (Dpp) signaling network underlying dorsal–ventral axis formation in flies. The absence of conservation for the roles of Bonus and TIF1-γ/TRIM33 reveals a shift in the dorsal–ventral patterning networks of flies and mice, systems that were previously considered wholly conserved. The shift occurred when the new gene TIF1-γ/TRIM33 replaced the function of the ubiquitin ligase Nedd4L in the lineage leading to vertebrates. Evidence of this replacement is our demonstration that Nedd4 performs the function of TIF1-γ/TRIM33 in flies during dorsal–ventral axis formation. The replacement allowed vertebrate Nedd4L to acquire novel functions as a ubiquitin ligase of vertebrate-specific Smad proteins. Overall our data reveal that the architecture of the Dpp/BMP dorsal–ventral patterning network continued to evolve in the vertebrate lineage, after separation from flies, via the incorporation of new genes.

Key words: **Bonus/TIF1/TRIM, Dorsal/NF-κB, Dpp/BMP/TGF-β, dorsal–ventral axis, embryonic development, *Drosophila*.**

Introduction

The classic model for the origin of new genes and their acquisition of novel functions is based on gene duplication; one copy of a pair of newly duplicated genes maintains the original function whereas the other copy accumulates mutations. Accumulation of deleterious mutations leads to a loss of function whereas accumulation of mutations conferring a selective advantage leads to a novel function and phenotypic evolution (Haldane 1933). The first empirical evidence for this model of new gene origination came from studies revealing that a duplication of the Bar locus effected eye phenotypes in *Drosophila* (Muller 1936).

Several recent studies have advanced our understanding of new gene origins, their influence on genetic systems (including developmental networks), and the resulting effects on phenotypic evolution. Regarding origins, a study in mouse embryonic stem cells revealing pervasive bidirectional transcription suggested to the authors that opposite strand transcription could provide a robust source for new genes (Almada et al. 2013; Wu and Sharp 2013). Regarding genetic systems, studies of new genes in *Drosophila* (those present in just a few species) showed that they can quickly become essential for viability, male fertility, and foraging behavior (Chen et al. 2010; Chen, Ni, et al. 2012; Chen, Spletter, et al. 2012). Indispensability for fertility and behavior was shown to result from the incorporation of new genes into existing networks and the reshaping of those networks to take maximum advantage of the new gene's novel function (Chen et al. 2013; Long et al. 2013). Detailed analysis of a new gene required for centromere integrity in *Drosophila* revealed that the rapid acquisition of essentiality is facilitated by a surprisingly small number of mutations (Ross et al. 2013).

Regarding development, two recent studies have expanded our understanding of the multifaceted nature of the evolution of development, a process for which a major focus of investigation was evolutionary conservation (e.g., *Hox* genes). A comparative analysis of the Hippo growth control pathway in mice and flies revealed that differences in pathway regulation were achieved via the gain and loss of function by pre-existing genes. This report demonstrates that the architecture of a vertebrate signaling pathway is not static but instead was impacted by the acquisition of new functions by existing genes after divergence from the lineage leading to flies (Bossuyt et al. 2014). A second study identified an example of a new gene-driven developmental switch leading to phenotypic evolution in the nematode genus *Pristionchus* (Ragsdale et al. 2013). Here, alternative forms of adult mouth morphology were found to be dependent upon the dosage of

Article

an often duplicated sulfatase that functions downstream of a pheromone sensing pathway. This indicated that gene duplication and the subsequent incorporation of the duplicates into a developmental network, even without neofunctionalization, can facilitate phenotypic diversity.

Developmental networks often employ morphogen gradient systems as a mechanism for regulating gene expression. In a morphogen gradient, secreted signaling molecules orchestrate distinct differentiation programs in target cells via concentration-dependent responses (Wolpert 1969). Among the best-understood gradients are the two that pattern the dorsal–ventral axis of the *Drosophila* embryo (Anderson 1998). First, activation of the transmembrane receptor Toll on the ventral side leads to a maternal ventralizing gradient of the transcription factor Dorsal with the highest level of Dorsal activity in the ventral-most region. Dorsal activates ventral-specific genes and modulates the expression of two signaling proteins; it represses *decapentaplegic* (*dpp*) and activates *short gastrulation* (*sog*). Second, extracellular interactions between Dpp and Sog then create a zygotic dorsalizing gradient of Dpp. The highest level of Dpp activity is in the dorsal-most region. Cells interpret the local concentration of Dpp along the dorsal–ventral axis via a pair of Smad signal transducers Mad and Medea and then adopt one of the five cell fates (O'Connor et al. 2006).

The reversal of dorsal–ventral polarity between insect and vertebrate embryos (insect "nerve cords" develop on the ventral side) is due to a zygotic ventralizing gradient of BMP that employs homologous proteins in same architecture and plays the same role as the Dpp dorsalizing gradient (Holley et al. 1995, 1996; De Robertis 2008). Recent studies identified a new component of the developmental network supporting the Dpp/BMP gradients that play a conserved role in flies and vertebrates. In both networks, the activities of the homologous signal transducers Medea and Smad4 are activated by the homologous deubiquitylases Fat facets (Faf) and USP9X (Dupont et al. 2009; Stinchfield et al. 2012). In vertebrates, an additional new participant was recently revealed; TIF1-γ/TRIM33 is a Ring class E-3 ubiquitin ligase that functions opposite USP9X by deactivating Smad4 and antagonizing BMP signaling (Dupont et al. 2005, 2012). The conservation of roles for Medea/Smad4 and Faf/USP9X formally requires an ubiquitin ligase for Medea; without a ligase there is no need for the Faf deubiquitylase. We wondered which *Drosophila* ubiquitin ligase performs the functions of TIF1-γ/TRIM33 in the Dpp dorsal–ventral signaling network?

Bonus is the *Drosophila* protein most closely related to TIF-γ/TRIM33. More precisely, Bonus is most closely related to four vertebrate members of a tightly linked subfamily within the TIF1/TRIM family: TIF1-α/TRIM24, TIF1-β/TRIM28, TIF-γ/TRIM33, and TIF-δ/TRIM66. The TIF1/TRIM family is a large and ancient one whose origins predate the diversification of metazoan animals, as shown by the presence of a TRIM37-like protein in a variety of protozoan species. The TIF-γ/TRIM33 subfamily is among the older subfamilies with a representative in all Bilaterian species (Marin 2012). To confirm subfamily age, our reciprocal Blast searches easily identified and confirmed a TIF-γ/TRIM33 family member in *Nematostalla vectensis*.

The connection between Bonus and the TIF-γ/TRIM33 subfamily is supported by experimental data. Studies of *bonus* mutants revealed activities as a nuclear receptor cofactor and as an inhibitor of βFTZ-F1-dependent transcription during metamorphosis (Beckstead et al. 2001, 2005). TIF1-α/TRIM24 interacts with retinoic acid and estrogen nuclear receptors, via the same LxxLL motif that mediates Bonus and βFTZ-F1 binding (Le Douarin et al. 1996). Side-by-side assays of Bonus and TIF1-β/TRIM28 in cultured cells identified a common role as a nuclear corepressor of c-Myb-dependent transcription (Nomura et al. 2004). A further parallel between Bonus and TIF1-β/TRIM28 is the ability to recruit the chromodomain protein HP1a to specific sites where together they alter chromatin configuration and modulate transcription (Nielsen et al. 1999; Ito et al. 2012).

We tested the hypothesis that Bonus has a conserved function as an ubiquitin ligase for Medea that serves as an antagonist of the Dpp dorsal–ventral network. We found that the role of Bonus is not the same as that of TIF1-γ/TRIM33 and instead the ubiquitin ligase Nedd4 does the job of TIF-γ/TRIM33 in Dpp signaling. Taken together our phylogenetic and developmental genetics data demonstrate that the architecture of the Dpp/BMP dorsal–ventral patterning network continued to evolve in the vertebrate lineage, after the separation from flies, via the incorporation of new genes.

Results

Birth Order of Vertebrate TIF1/TRIM Subfamily Members Most Closely Related to Bonus

To better characterize the relationship between Bonus, TIF1-γ/TRIM33 and other vertebrate subfamily members we conducted a series of phylogenetic studies. First, we created a set of six small trees that utilized 11 sequences from humans, flies, and nematodes that share multiple structural domains with Bonus (see supplementary table S1, Supplementary Material online, for accession numbers and supplementary table S2, Supplementary Material online, for domain comparisons). In our view employing just these sequences has three benefits: 1) the alignments contain a large number of informative sites, 2) the resulting trees can be easily compared with trees from the TGF-β, Wnt, and Hippo pathways (e.g., Newfeld et al. 1999; Konikoff et al. 2010; Wisotzkey et al. 2012) and 3) flies and nematodes provide the ability to experimentally evaluate the functional consequences of sequence divergence.

We then created a set of six larger trees employing 47 sequences. These included an additional 36 that we identified in species that lie taxonomically between nematodes and humans. We added sequences from four additional vertebrate species (mouse, chicken, zebrafish, and pufferfish) as well as four species from groups that are regarded as vertebrates' closest relatives (cephalochordates, echinoderms, urochordates, and hemichordates). We also included three lophotrocozoan species (two annelids and a sea slug) to fill the large evolutionary gap between nematodes/flies and vertebrates/chordates. The alignments underlying these trees

had fewer informative sites leading to lower resolution but nevertheless revealed important insights on the origin of the Bonus-TIF1-γ/TRIM33 subfamily.

Initial alignments with the 11 sequences revealed that the current sequence of human TIF1-δ/TRIM66 corresponds to the shorter mouse TIF1-δ/TRIM66 isoform2 that does not contain a RING domain. Given that the RING domain is a canonical feature of the TIF1/TRIM family (Boudinot et al. 2011), we predicted and then identified a human TIF1-δ/TRIM66 isoform1 that contains this domain (supplementary figs. S1–S4, Supplementary Material online). We employed this extended sequence, that we named TIF1-δ*/TRIM66, in our analysis.

We included vertebrate TRIM71 proteins as they belong to a distinct TIF1/TRIM subfamily (SubgroupD; Sardiello et al. 2008). SubgroupD also contains two fly proteins (DmMei-P26 and DmBrat) and two nematode proteins (CeNHL-2 and CeNCL-1). The SubgroupD sequences provided an important second subfamily for our trees that aided in interpreting the placement of nonmodel organism sequences. We utilized three distinct algorithms (Neighbor Joining, Maximum Likelihood, and Bayesian) to generate trees and each was rooted with two carefully chosen outgroups. We employed CeBET-2 as an outgroup in half of our trees because it contains only two Bromo domains (one of the five types of structural domain found in TRIM family members; supplementary table S2, Supplementary Material online). We utilized HsTRIM37 as an outgroup in the other half because this protein never clustered with any other human TRIM protein (Sardiello et al. 2008). Features common to many trees engender the most confidence.

All trees (fig. 1 and supplementary fig. S5, Supplementary Material online) support the previously reported subfamily of Bonus with four vertebrate TIF1/TRIM sequences (SubgroupC; TIF1-α/TRIM24, TIF1-β/TRIM28, TIF1-γTRIM33, and TIF1-δ/TRIM66; Sardiello et al. 2008). Examination of branch topology and length as well as node confidence in our trees supports the hypotheses that human TIF1-α/TRIM24 and TIF1-γ/TRIM33 resulted from the most recent duplication in this cluster. These two sequences cluster together in all trees and always have the shortest branches. Eleven of our 13 trees provide strong statistical support for this cluster with bootstrap or posterior probabilities above 90%. In addition, two trees in Sardiello et al. (2008) display 100% bootstrap confidence in this cluster (their figs. 4*C* and 6*B*). Taking a step back, the data suggest that TIF1-β/TRIM28 is the progenitor of this pair via an older duplication; it is linked to them in seven trees whereas TIF1-δ*/TRIM66 is linked to them in three (two of our trees have TIF1-β/TRIM28 and TIF1-δ*/TRIM66 clustered).

Identifying the oldest vertebrate subfamily member proved more complicated as TIF1-β/TRIM28 and TIF1-δ*/TRIM66 show a variety of relationships to Bonus. TIF1-δ*/TRIM66 maps closest in eight trees and TIF1-β/TRIM28 closest in four trees. However, TIF1-β/TRIM28 has the longest branch in eight trees and TIF1-δ*/TRIM66 the longest in four trees. In this regard, we noted that the paper reporting the cloning and characterization of mouse TIF1-δ/TRIM66, the only paper describing its expression in any species, states that this gene is testis-specific (Khetchoumian et al. 2004). Thus, it seems likely that distinct selective pressures on germline-exclusive genes led this protein to accumulate amino acid changes at a rate exceeding those of its somatically expressed siblings. As a result, it moved from its expected position to one of the greater divergence and branch length in a subset of trees. Taken together one hypothesis we favor is that TIF1-β/TRIM28 is the oldest human family member and the most similar to Bonus; TIF1-β/TRIM28 gave rise first to TIF1-δ*/TRIM66 and then to the original member of the TIF1-α/TRIM24 and TIF1-γTRIM33 pair.

Completing the larger picture of this subfamily in vertebrates, we noted that TIF1-β/TRIM28 was lost in the lineage leading to fish whereas TIF1-α/TRIM24 experienced a duplication in pufferfish. In contrast to the four subfamily members present in all vertebrates except fish, all nonvertebrate species contain a single family member. Thus, the three rounds of duplication that led from TIF1-β/TRIM28 to TIF1-γ/TRIM33 occurred in the common ancestor of all vertebrates but after the divergence from their closest nonvertebrate relatives. This scenario of frequent duplication and subsequent lineage-specific deletion is visible throughout the TRIM family (Marin 2012). As a result, there are 66 members in humans (Sardiello et al. 2008) with a mix of common and unique family members among the 55 zebrafish and 44 pufferfish family members (Boudinot et al. 2011).

To identify the newest vertebrate subfamily member, either TIF1-α/TRIM24 or TIF1-γ/TRIM33, we relied on three lines of evidence. Each of these supports the hypothesis that TIF1-γ/TRIM33 is the newest. First, TIF1-γ/TRIM33 has the shortest branch in 9 of 12 trees. Second, TIF1-γ/TRIM33 does not contain an HP1-interacting PxVxL sequence (fig. 1E). This interaction is conserved in Bonus via a similar PxVxI motif (Nielsen et al. 1999; Ito et al. 2012). Third, domain comparisons indicate that TIF1-γ/TRIM33 never shows the greatest identity or similarity to Bonus (supplementary table S3 and fig. S6, Supplementary Material online). Taken together these criteria support the hypothesis that TIF1-γ/TRIM33 is the most evolutionarily distant from Bonus and thus the newest vertebrate subfamily member. This designation is consistent with reports that TIF1-γ/TRIM33 functions primarily as a monoubiquitin ligase, a role not frequently associated with its siblings (Deshaies and Joazeiro 2009). The best-characterized role of TIF1-γ/TRIM33 is as an antagonist of the BMP signaling network during dorsal–ventral axis formation (Dupont et al. 2005, 2009; Morsut et al. 2010; Agricola et al. 2011).

Notwithstanding our hypothesis that TIF1-β/TRIM28 is the oldest vertebrate member of the subfamily, the pattern of conservation between Bonus and its four vertebrate relatives is uneven. None of the vertebrate proteins was the most identical or the most similar to Bonus in more than two of the six structural domains. Further, in two domains, the vertebrate protein with the highest identity to Bonus did not have the highest similarity (e.g., greatest identity in the BBC domain is TIF1-β/TRIM28 but greatest similarity is TIF1-δ*/TRIM66; supplementary table S3, Supplementary Material online).

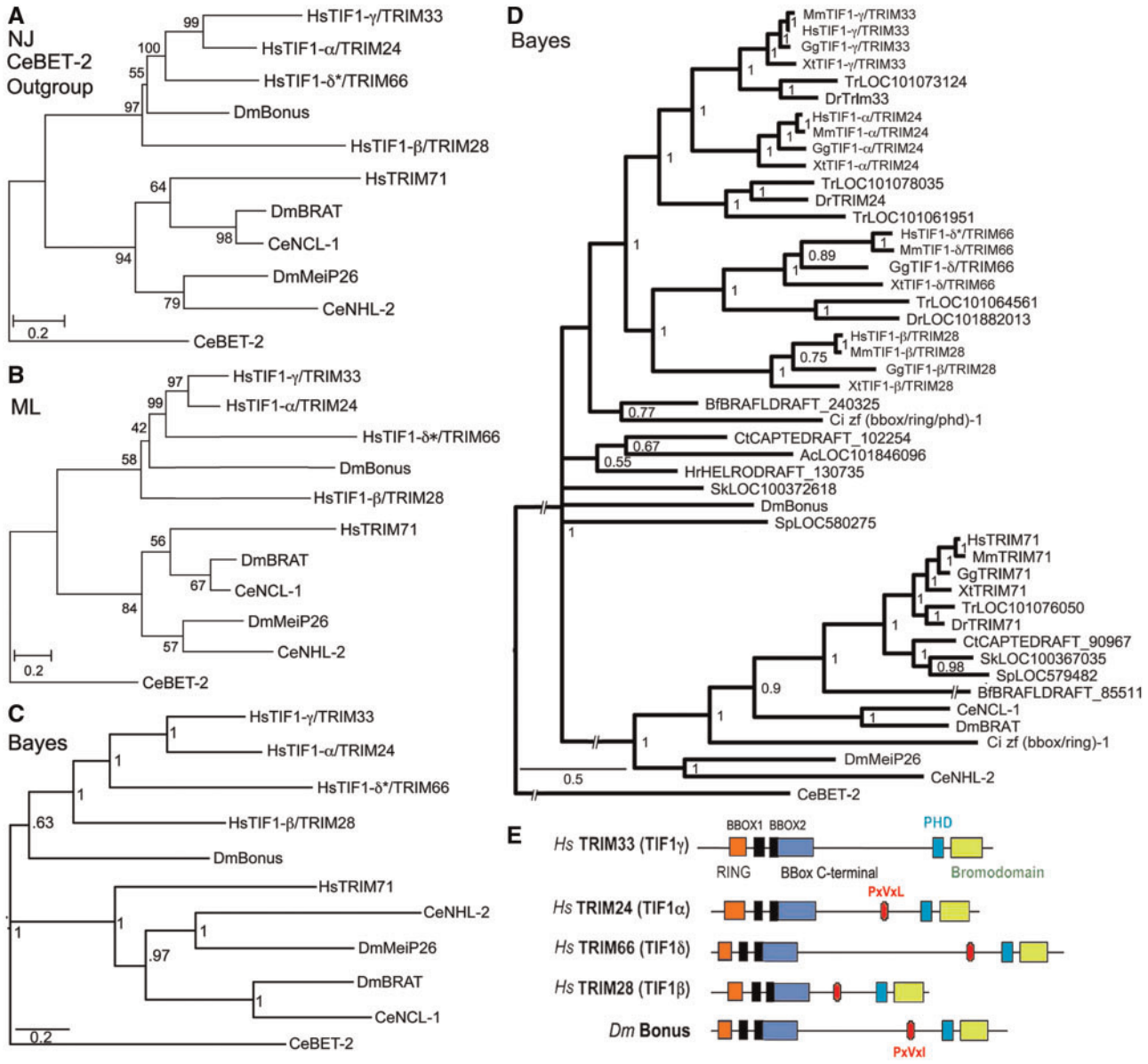

FIG. 1. Phylogenetic relationships and structure of Bonus-Tif1-γ/TRIM33 subfamily members. (*A*) Neighbor Joining (NJ), (*B*) Maximum Likelihood (ML) and (*C*) Bayesian trees of ten human (Hs), fly (Dm), and nematode (Ce) TRIM family sequences related to Bonus. Accession numbers are in supplementary table S1, Supplementary Material online. HsTRIM71 was chosen to anchor the non-Bonus fly and nematode sequences into a single subfamily based on Sardiello et al. (2008). CeBET-2 was chosen as the outgroup because it does not belong to the TRIM family and shares only the BROMO of the five structural domains shared by the others. The alignment contained 551 informative positions. A scale bar showing amino acid substitutions per site is present. Bootstrap values (NJ and ML trees) above 40% and posterior probabilities above 0.5 (Bayesian tree) are shown. Bootstrap values above 70% and posterior probabilities above 0.95 are considered statistically significant. Each tree contains the same two distinct subfamilies. Within one subfamily, Bonus is either the most distant sequence or between TIF1-β/TRIM28 and TIF1-δ/TRIM61, whereas TIF1-γ/TRIM33 and TIF1-α/TRIM24 consistently group together. (*D*) Expanded Bayesian tree containing all 47 sequences in supplementary table S1, Supplementary Material online, derived from an alignment with 173 informative positions. The same two statistically supported subfamilies are visible. The topology of the Bonus-TIF1-γ/TRIM33 subfamily is a slightly different from the other trees. The four vertebrate sequences resolve into two clusters with Bonus a distant outlier. (*E*) Schematic comparison of the domain structure of Bonus-TIF1-γ/TRIM33 subfamily proteins. The locations of seven distinct domains are shown: RING, orange; BBOX, black (2); BBox C-terminal, blue; PxVxL (or the biochemically similar PxVxI in Bonus), red; PHD, aqua; and BROMO, green.

Thus, it was conceivable that Bonus, as the only subfamily member in flies, was capable of functioning similarly to any of the vertebrate proteins including TIF1-γ/TRIM33. We then tested the hypothesis that Bonus serves as an ubiquitin ligase for Medea that antagonizes the Dpp signaling network during dorsal–ventral axis formation in *Drosophila*.

bonus Zygotic Nuclear Requirement for Dpp Responsiveness

Initial studies of embryonic cuticles revealed that two *bonus* zygotic mutant genotypes displayed defects in dorsal–ventral patterning. Eighteen percent of $bonus^{487}/bonus^{21B}$ and 13%

of $bonus^{21B}/bonus^{EY1763}$ cuticles were partially ventralized (see Materials and Methods for descriptions of alleles). The most severely affected individuals resembled dpp^{hr4} cuticles and cuticles generated by $Medea^{15}$ females (fig. 2 and supplementary table S4, Supplementary Material online). Further, heterozygosity for $bonus^{21B}$ partially rescued dorsalization defects due to hemizygosity for sog^{yl26} (supplementary table S5 and fig. S7, Supplementary Material online). This effect is also seen with dpp^{hr4}, $Medea^{15}$, and faf^{B6} (Stinchfield et al. 2012). These data suggest that Bonus plays an instructive role in dorsal–ventral patterning, a role not predicted by analogy to TIF1-γ/TRIM33. If Bonus were a ubiquitin ligase for Medea, then *bonus* zygotic mutants would be dorsalized due to reduced Medea ubiquitylation and hyperactive Dpp signaling.

We then adjusted our model for Bonus function by incorporating a different target. In the new hypothesis, Bonus serves as a Toll pathway ubiquitin ligase. Here, the prediction is that loss of Bonus ubiquitin ligase activity will lead to Toll hyperactivation, expansion of Dorsal, increased repression of Dpp, and ventralization of the embryo. We examined this hypothesis in $bonus^{21B}/bonus^{EY1763}$ embryos stained with Bonus antibody.

Dorsal protein shows normal ventral nuclear accumulation at stage 5 in *bonus* mutants (fig. 3*A*–*D*). To confirm this result, we examined pMad expression as a marker of Dpp pathway activity. In wild type, at stage 5, pMad is present as a narrow stripe in the dorsal-most region reflecting the concentration of Dpp there via extracellular transport by Sog. dpp^{hr4} mutants have a point mutation that interferes with transport and thus display reduced dorsal pMad accumulation in a background of diffuse staining. $Medea^{15}$ maternal mutants show normal pMad due to the loss of signaling downstream of Mad phosphorylation. *bonus* zygotic mutants have normal pMad as well (fig. 3*E*–*H*). Thus, Bonus does not antagonize either of these pathways.

These experiments also showed that at stage 5, Bonus is a ubiquitous nuclear protein. Thus, we then hypothesized that *bonus*'s positive role in dorsal–ventral patterning was associated with the regulation of Dpp responsiveness. To test this, we analyzed Hindsight expression in stage 10 embryos. Hindsight is a marker for the amnioserosa, the dorsal-most tissue and the one that requires the highest level of Dpp signaling (Ray et al. 1991). Roughly 17% of $bonus^{21B}/bonus^{EY1763}$ embryos displayed severely reduced Dpp-dependent Hindsight expression in the amnioserosa (fig. 3*I*–*L*) consistent with the frequency of cuticle defects in this genotype. Individuals of this genotype contained normal Dpp-independent Hindsight expression in the foregut and hindgut (supplementary fig. S8, Supplementary Material online). Data from *bonus* mutants, together with Bonus nuclear localization after stage 5 and documented roles in chromatin remodeling (Beckstead et al. 2001), are consistent with a zygotic nuclear requirement for Bonus in dorsal–ventral patterning as a modulator of Dpp responsiveness.

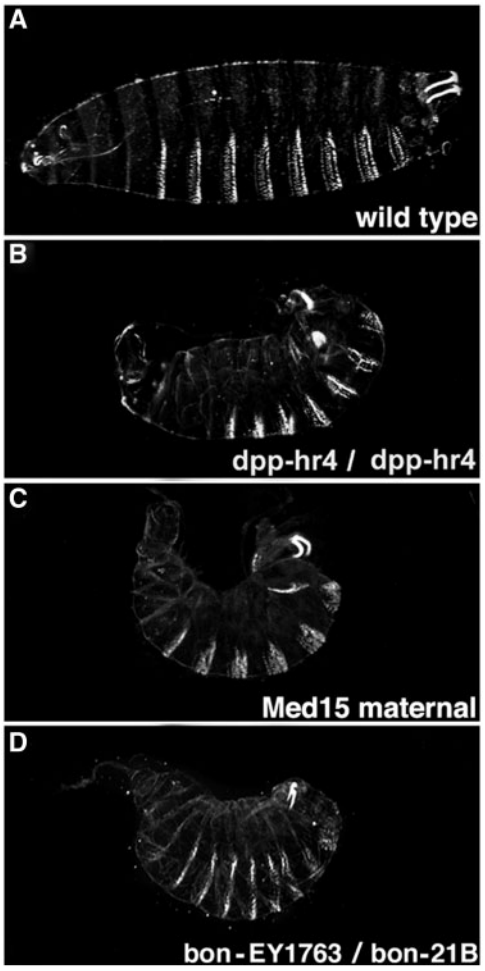

FIG. 2. *bonus* zygotic mutants phenocopy *dpp* mutants. Cuticles in lateral view with anterior to the left and dorsal up. The maternally contributed allele is listed first. The molecular lesion in each mutant is described in the Materials and Methods. (*A*) Wild type. The broad white denticle belts on the ventral surface (bottom), narrow white Filzkorper in the posterior spiracles (upper right corner) and internal head skeleton (left side) are visible. (*B*) Homozygous dpp^{hr4} ventralized cuticle with a short curved body, dorsally extended denticles, herniated head, and defective Filzkorper. (*C*) Homozygous maternal $Medea^{15}$ ventralized cuticle is similar to dpp^{hr4}. (*D*) $bonus^{EY1763}/bonus^{21B}$ transheterozygous ventralized cuticle is also similar to dpp^{hr4}.

Bonus and Dorsal Nuclear Translocation Is Synchronous in Multiple Genotypes

The nonconservation of zygotic *bonus* function in the Dpp dorsal–ventral signaling network with that of TIF1-γ/TRIM33 in the BMP dorsal–ventral signaling network did not preclude the possibility that a maternal Bonus function could be conserved. Examination of unfertilized eggs showed that Bonus is maternally loaded and cytoplasmic (supplementary fig. S9A′–A‴, Supplementary Material online). As Bonus is ubiquitously nuclear by stage 5 (e.g., fig. 3*A*), we tested the hypothesis that Bonus nuclear translocation occurs between mitotic cycles 9 and 12, the stages when Dorsal (cycle 9) and pMad (cycle 12) enter the nucleus in response to their respective signals (Roth et al. 1989; Steward 1989; Shimmi et al. 2005). We examined wild type as well as Toll maternal

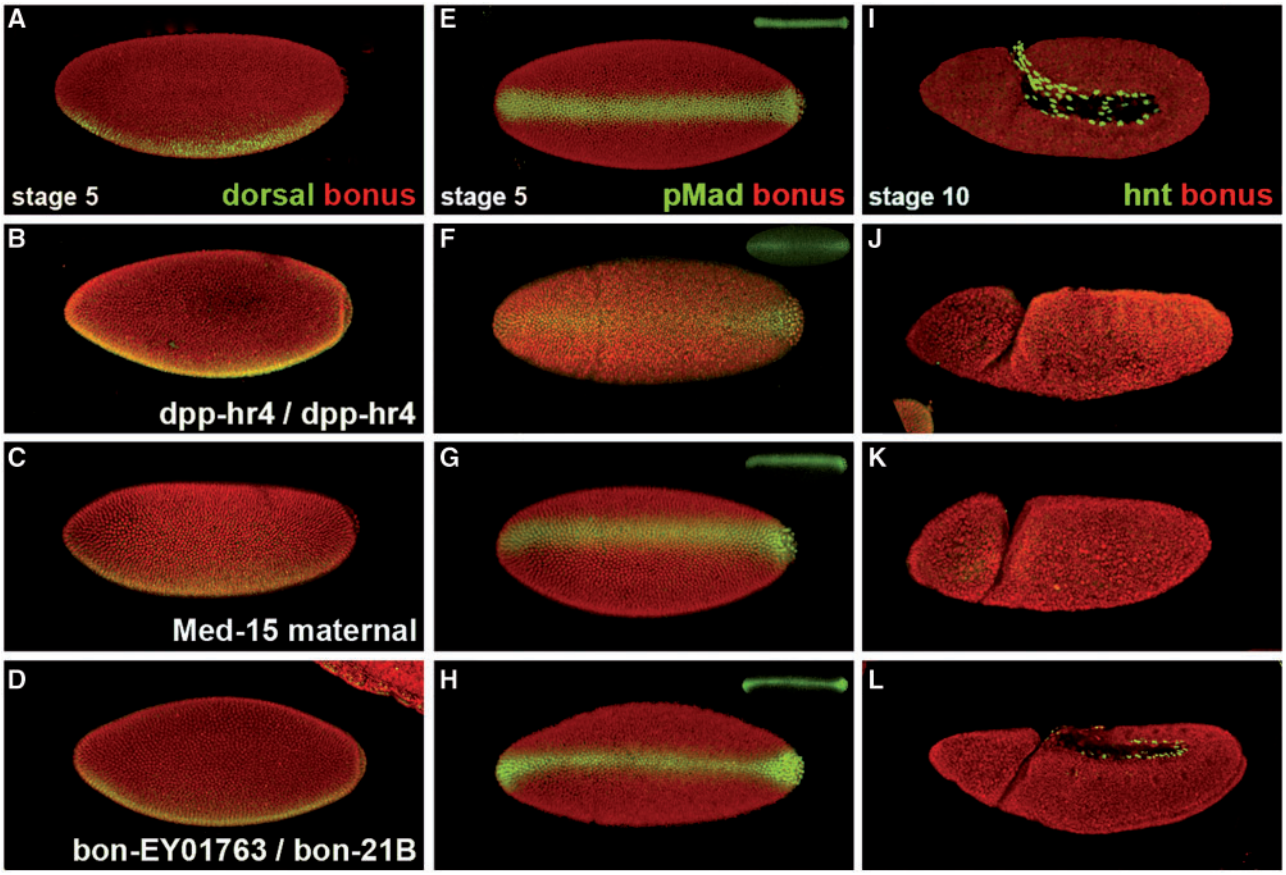

Fig. 3. *bonus* zygotic requirement for Dpp responsiveness. (*A*–*D*) Stage 5 embryos (nuclear cycle 14) in lateral view displaying Bonus (red) and Dorsal (green). (*E*–*H*) Stage 5 embryos in dorsal view displaying Bonus (red) and pMad (green) with pMad alone as an inset. (*I*–*L*) Stage 10 embryos in lateral view with Bonus (red) and Hindsight (green). (*A*, *E*, *I*) Wild type embryos with ubiquitous nuclear Bonus, ventral Dorsal nuclear stripe, sharp dorsal pMad nuclear stripe, and nuclear Hindsight in amnioserosa cells. (*B*, *F*, *J*) dpp^{hr4} homozygous embryo with normal nuclear Bonus and Dorsal. The pMad dorsal stripe is expanded with diffuse pMad throughout the embryo. Hindsight is absent. (*C*, *G*, *K*) Embryo from a homozygous $Medea^{15}$ female with normal Bonus, Dorsal, and pMad but no Hindsight. (*D*, *H*, *L*) $bonus^{EY1763}/bonus^{21B}$ embryo has normal nuclear Bonus, Dorsal, and pMad but significantly reduced Hindsight.

gain and loss of function embryos to test the hypothesis that this pathway influences Bonus nuclear translocation.

In wild type at cycle 8, the last cycle of strictly maternal expression (Pritchard and Schubiger 1996), Bonus and Dorsal are wholly cytoplasmic. The maternal to zygotic transition begins during cycle 9 and in wild type embryos Bonus becomes ubiquitously nuclear. At the same time, Dorsal becomes nuclear within the ventral-most 40% of nuclei whereas remaining cytoplasmic elsewhere. The maternal-to-zygotic transition is complete during stage 10 and in wild type embryos Bonus and Dorsal maintain their respective subcellular locations through cycle 14 (fig. 4*A*–*G*; left column with high magnification views in supplementary fig. S9*B*–*D*, Supplementary Material online).

$Toll^{r4}$ is a loss of function allele with modest haploinsufficiency (Anderson, Bokla, et al. 1985; Anderson, Jürgens, et al. 1985). In embryos from $Toll^{r4}$ heterozygous mothers, Bonus and Dorsal are wholly cytoplasmic at stage 8 and then their nuclear translocation is delayed. During cycles 9 and 10, ubiquitous cytoplasmic expression of both proteins persists. In cycle 11, they begin nuclear translocation with normal spatial parameters. During cycles 12 and 13, they become increasingly nuclear until the wild type pattern appears at cycle 14, a delay of four nuclear cycles (fig. 4*A*′–*G*′; middle column). $Toll^{8}$ is strong gain of function allele (Anderson, Bokla, et al. 1985; Anderson, Jürgens, et al. 1985). In embryos from $Toll^{8}$ heterozygous mothers, Bonus and Dorsal are wholly cytoplasmic at stage 8. They then become ubiquitously nuclear during cycle 9 and maintain this pattern through cycle 14 (fig. 4*A*″–*G*″; right column). In all genotypes, Bonus and Dorsal translocate to the nucleus synchronously.

bonus Maternal Cytoplasmic Requirement for Dorsal Nuclear Translocation

Given this synchrony, we then examined Dorsal nuclear localization in embryos without Bonus derived from $bonus^{21B}$ germline clone bearing females. We mated these females to heterozygous $bonus^{21B}$ males. Germline clone eggs are maternally hemizygous for the *bonus* mutation. Germline clone embryos can be either zygotically homozygous or zygotically heterozygous for $bonus^{21B}$ depending upon the paternally contributed chromosome. $bonus^{21B}$ deletes the normal initiator methionine (Beckstead et al. 2001) and thus a reduction

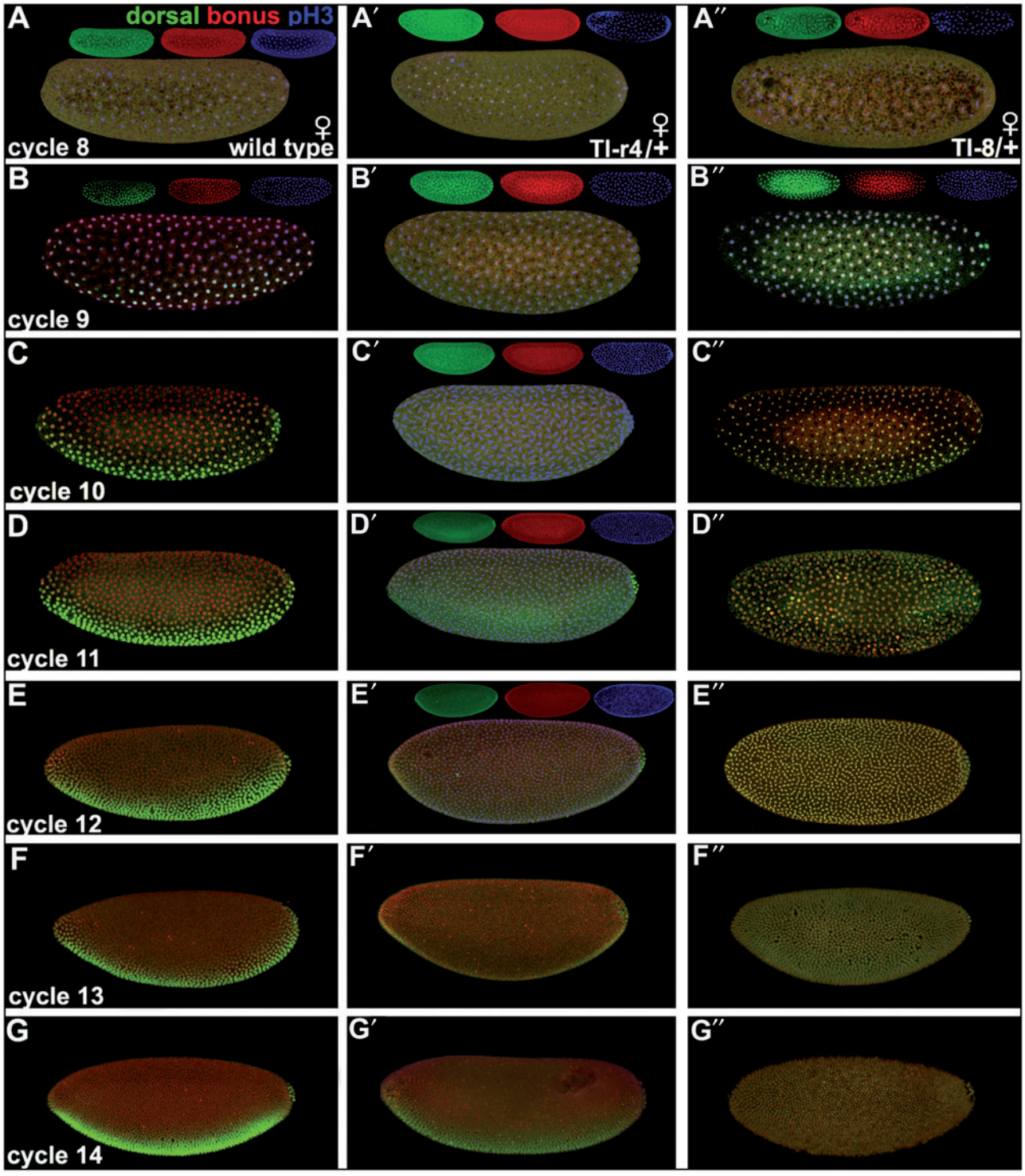

Fig. 4. Synchronous nuclear translocation of Bonus and Dorsal. Embryos in lateral view in mitotic cycles 8–14. Mothers were wild type (*A*–*G*), *Toll*^{r4}/ + (*A*′–*G*′), and *Toll*^{8}/ + (*A*″–*G*″) mated to wild type fathers. The molecular lesion in each *Toll* mutant is described in the Materials and Methods. Embryos display Bonus (red), Dorsal (green), and the mitotic marker pH3 (blue) for cycles 8 and 9 (wild type and *Toll*^{8}) or cycles 8–12 (*Toll*^{r4}). For three-color images, each channel is also shown as an inset. The remaining images display only Bonus (red) and Dorsal (green). Left column: Wild type. (*A*) Cycle 8: pH3 is ubiquitously nuclear with Bonus and Dorsal ubiquitously cytoplasmic. (*B*–*G*) Cycles 9–14: Bonus is ubiquitously nuclear with Dorsal visible within the ventral-most 40% of nuclei while remaining cytoplasmic elsewhere. High magnification views of nuclei in cycles 8–10 embryos are shown in supplementary figure S9, Supplementary Material online. Middle column: *Toll*^{r4}/ + . (*A*′–*C*′) Cycles 8–10: Bonus and Dorsal are ubiquitously cytoplasmic. (*D*′) Cycle 11: Bonus shows a mixture of ubiquitiously cytoplasmic and weak nuclear expression. Dorsal is also mixed with primarily cytoplasmic and weak nuclear expression in the ventral-most 40%. (*E*′) Cycle 12: Increasing ubiquitous nuclear and diminished cytoplasmic Bonus. Dorsal shows increasing nuclear expression in the ventral-most 40% with cytoplasmic expression elsewhere. (*F*′, *G*′) Cycles 13 and 14: Roughly wild type expression of Bonus and Dorsal. Right column: *Toll*^{8}/ + . (*A*″) Cycle 8: Bonus and Dorsal are ubiquitously cytoplasmic. (*B*″–*G*″) Cycles 9–14: Bonus and Dorsal are ubiquitously nuclear.

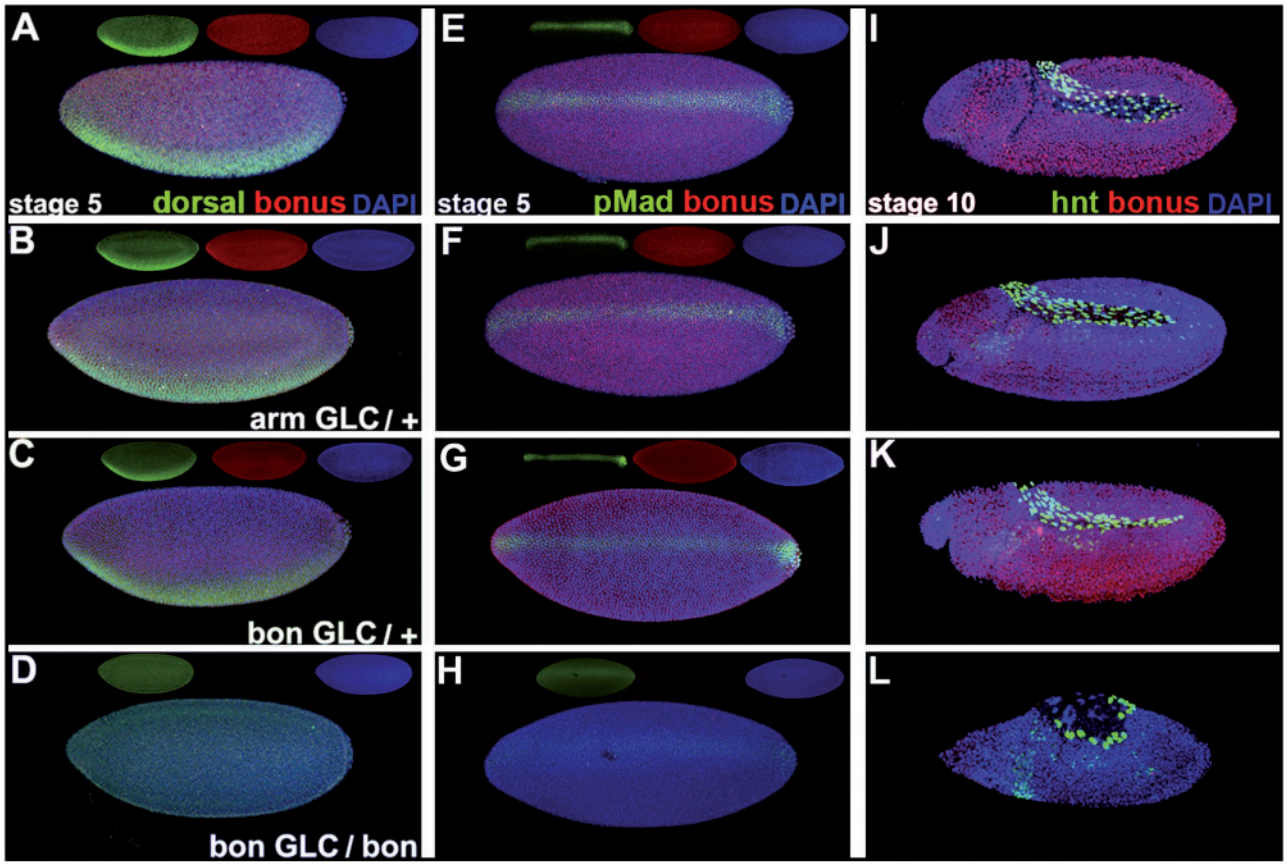

Fig. 5. *bonus* maternal requirement for Dorsal nuclear translocation. (*A*–*D*) Stage 5 embryos in lateral view displaying Bonus (red), Dorsal (green), and the DNA dye DAPI (blue) plus individual channels as insets. (*E*–*H*) Stage 5 embryos in dorsal view with Bonus (red), pMad (green), and DAPI (blue) plus insets. (*I*–*L*) Stage 10 embryos in lateral view with Bonus (red), Hindsight (green), and DAPI (blue). (*A*, *E*, *I*) Wild type embryos show ubiquitiously nuclear Bonus, ventral Dorsal nuclear stripe, sharp dorsal pMad nuclear stripe, and Hindsight in amnioserosa cells. (*B*, *F*, *J*) arm-lacZ germline clone embryos display normal Bonus, Dorsal, pMad, and Hindsight. (*C*, *G*, *K*) Heterozygous $bonus^{21B}$ germline clone embryos with paternal rescue display normal Bonus, Dorsal, pMad, and Hindsight. (*D*, *H*, *L*) Homozygous $bonus^{21B}$ germline clone embryos with no paternal rescue were identified via reduction of Bonus expression. These embryos display no visible nuclear Dorsal, faint ventrally expanded dorsal pMad stripe with diffuse pMad background, and significantly reduced Hindsight in amnioserosa cells.

of wild type Bonus expression identified the zygotically homozygous $bonus^{21B}$ embryos. In this experiment, we can distinguish maternal from zygotic requirements for Bonus in embryonic development.

At stage 5, wild type, arm-lacZ germline clone embryos (a control for the method) and zygotically heterozygous $bonus^{21B}$ germline clone embryos display normal Dorsal expression. Zygotically homozygous $bonus^{21B}$ germline clone embryos show no visible nuclear Dorsal (fig. 5*A*–*D*). This reveals a maternal cytoplasmic requirement for *bonus* in Dorsal nuclear translocation. Without any nuclear Dorsal $bonus^{21B}$ germline clone embryos should be fully dorsalized due to loss of Dorsal repression of *dpp* ventrally and the absence of Dorsal activation of Sog. Consistent with this prediction, homozygous $bonus^{21B}$ germline clone embryos display ventrally expanded pMad nuclear accumulation barely above a background of ubiquitous expression (fig. 5*E*–*H*). This observation is supported by *dpp* in situ hybridization studies in these embryos revealing ventral expansion of Dpp transcription. The presence of any pMad nuclear accumulation, in embryos without visible Dorsal nuclear translocation, may be explained by the presence of a cryptic methionine in the portion of *bonus* exon1 that is not deleted in $bonus^{21B}$ (supplementary fig. S10, Supplementary Material online). $bonus^{21B}$ may not be a protein null allowing invisible but functional amounts of Dorsal into the nucleus and the slight dorsal–ventral pMad polarity seen in homozygous $bonus^{21B}$ germline clone embryos.

The absence of Dorsal nuclear translocation and subsequent reduction in pMad nuclear accumulation are inconsistent with the loss of Hindsight expression in the amnioserosa at stage 10 observed in homozygous $bonus^{21B}$ germline clone embryos (fig. 5*I*–*L*). If *bonus* has no effect on dorsal–ventral patterning beyond the maternal cytoplasmic requirement for Dorsal nuclear translocation, then $bonus^{21B}$ germline clone embryos should be almost completely dorsalized. Dorsalized embryos display expanded Hindsight. To confirm this prediction, we examined the effect of reduced Dorsal nuclear accumulation on Hindsight expression in embryos derived from $Toll^{r3}/Toll^{r4}$ females. This temperature-sensitive genotype has severely, but not completely, compromised *Toll* signaling (Schneider et al. 1991). In embryos from these

females, pMad nuclear accumulation and Hindsight amnioserosa expression are both ventrally expanded (supplementary fig. S11, Supplementary Material online). Homozygous *bonus*^{21B} germline clone embryos display roughly the same effect on pMad as *Toll*^{r3}/*Toll*^{r4} (supplementary fig. S12, Supplementary Material online) but they display the opposite effect on Hindsight. In homozygous *bonus*^{21B} germline clone embryos Hindsight expression is instead consistent with that seen in *bonus* zygotic mutant embryos, reflecting a distinct zygotic nuclear requirement in Dpp responsiveness.

Discussion

Bonus Contributes to Two Embryonic Dorsal–Ventral Patterning Networks

From a developmental perspective, the data reveal that *bonus* plays two distinct roles in dorsal–ventral axis formation. There is a maternal cytoplasmic role in Toll signaling required for Dorsal nuclear accumulation and there is a zygotic nuclear role downstream of pMad required for Dpp responsiveness. The latter fits squarely within the existing paradigm for TIF1/TRIM proteins in chromatin remodeling and transcription regulation. TIF1/TRIM proteins, including Bonus, interact directly via their PxVxL/I domains with members of the HP1 family to promote the modulation of gene expression (Le Douarin et al. 1996; Nielsen et al. 1999; Beckstead et al. 2001). Perhaps the PxVxI motif in Bonus facilitates Dpp responsiveness via interactions with its signal transducers Mad, Medea, or Schnurri.

Regarding the maternal role, the presence of a near-perfect match in Dorsal to the AF2-AD consensus sequence (supplementary fig. S13, Supplementary Material online) suggests that this function may also be mediated by a TIF1/TRIM family paradigmatic mechanism. In this case, Bonus and TIF1/TRIM proteins employ their LxxLL motif to bind the AF2-AD consensus sequence in βFTZ-F1 (Beckstead et al. 2001) or nuclear hormone receptors (Le Douarin et al. 1996). We determined that there is no AF2-AD sequence in Cactus, the protein that sequesters Dorsal in the cytoplasm further suggesting that Bonus regulation of Dorsal nuclear translocation may be direct. Perhaps this interaction is necessary because several reports suggest that release from Cactus is insufficient for Dorsal nuclear translocation. For example, the phosphorylation of Dorsal is also required (Whalen and Steward 1993; Drier et al. 1999). Thus, one potential function for Bonus may be to facilitate Dorsal phosphorylation. Alternatively, Bonus may act as a chaperone to help Dorsal efficiently locate its targets during the rapid nuclear cycles 8, 9, and 10. We propose that the ability of Bonus to translocate to nuclei throughout the embryo, rather than only ventrally like Dorsal, is due to its ability to respond to lower doses of Toll signaling than Dorsal. This scenario is similar to the differential responses of *spalt* (narrow response to high concentrations) and *optomotor blind* (wide response to high and low concentrations) to the Dpp gradient in third instar wing imaginal discs (O'Connor et al. 2006).

Acquisition of Nedd4 Function by TIF1-γ/TRIM33 during Vertebrate Evolution

From an evolutionary perspective, the analyses showed that vertebrates' closest relatives have only a single Bonus-TIF1-γ/TRIM33 subfamily sequence. A preponderance of the phylogenetic data suggests that TIF1-β/TRIM28 is most similar to the common ancestor of the four vertebrate subfamily members. Then during the vertebrate whole-genome duplication TIF1-δ/TRIM66 was created and diverged significantly. Subsequently, but prior to the divergence of fish, TIF1-β/TRIM28 generated TIF1-α/TRIM24 and then TIF1-α/TRIM24 generated TIF1-γ/TRIM33. After the divergence of fish but before the split between zebrafish and pufferfish the gene for TIF1-β/TRIM28 was lost in the fish lineage.

Thus, our demonstration that the role of the newest subfamily member TIF1-γ/TRIM33 as an ubiquitin ligase for Smad4 is not conserved for Bonus and Medea begs the question, who does this job in flies? There must be an ubiquitin ligase for Medea that complements the role of the conserved deubiquitylase Faf in Dpp dorsal–ventral signaling. We eliminated the ubiquitin ligase dSmurf (known as Lack in Flybase) even though it is a well-known antagonist of Dpp dorsal–ventral signaling (Podos et al. 2001). dSmurf was explicitly shown to target Mad but not Medea (Liang et al. 2003). Another candidate is Highwire (Hiw), an ubiquitin ligase for Medea at the larval neuro-muscular junction (McCabe et al. 2004). A third candidate is Nedd4, the only fly member of a HECT class E-3 ubiquitin ligase family and homolog of Nedd4L that antagonizes Smad activity during TGF-β signaling in mammals (Alarcón et al. 2009; Gao et al. 2009; Aragón et al. 2011). To date Nedd4 has not been connected to TGF-β signaling in *Drosophila*.

We examined the ability of the latter candidates to suppress the roughly 40% haploinsufficiency associated with *dpp*^{hr27} (Wharton et al. 1993). The logic was that an excess of maternally provided, nonubiquitylated Medea will amplify the weak Dpp signal associated with this allele. Maternal homozygosity for two *hiw* alleles had no effect, consistent with reports that *hiw* mRNA is not visible in unfertilized eggs (Wan et al. 2000). Maternal heterozygosity for either *nedd4*^{DG05310} or *nedd4*^{T119FS} (Huet et al. 2002; Sakata et al. 2004) dominantly suppressed *dpp*^{hr27} haploinsufficiency at roughly the same rate as *smurf*^{KG07014} (supplementary table S6, Supplementary Material online). This is consistent with reports that *nedd4* mRNA is maternally loaded (Tadros et al. 2007) and suggests that Nedd4 is the Medea ubiquitin ligase functioning opposite Faf in Dpp dorsal–ventral patterning.

One explanation for Bonus nonconservation is that the ubiquitylation role for TIF1-γ/TRIM33 is derived. After the amplification of the TIF1/TRIM family in the lineage leading to vertebrates, the newest member TIF1-γ/TRIM33 accumulated sufficient mutations to become an effective Ring class ubiquitin ligase. Supporting this hypothesis, expression of *Xenopus* TIF1-γ/TRIM33 in fly wings generates vein defects consistent with a role as a Medea ubiquitin ligase and these defects are suppressed by coexpression of Faf (Dupont et al. 2009). Then after becoming an ubiquitin ligase, TIF1-γ/

TRIM33 did not assume a novel role that would confer a selective advantage as predicted by the classical model of new gene evolution by gene duplication. Instead TIF1-γ/TRIM33 assumed the role in dorsal–ventral patterning performed by the existing gene Nedd4L as a Smad4 ubiquitin ligase. Perhaps the selective advantage of this replacement is that the RING class TIF1-γ/TRIM33 is more efficient then the HECT class Nedd4L as a Smad4 ubiquitin ligase. Thus, Nedd4L became free to assume a novel function.

Phylogenetic analyses of the TGF-β family (Kahlem and Newfeld 2009) and the Nedd4 family (supplementary fig. S14, Supplementary Material online) support this view. The TGF-β/Activin/Nodal subfamily that employs Smad2/Smad3 signal transducers expanded from 4 in flies to 14 during vertebrate evolution. Alternatively, there is just a pair of Nedd4 proteins in vertebrates and sequence similarity to *Drosophila* Nedd4 indicates that Nedd4L is the ancestral form (supplementary table S7, Supplementary Material online). Notwithstanding its close relationship to fly Nedd4, Nedd4L specifically targets Smad3 and Smad7, two vertebrate-specific Smads (Aragón et al. 2011, 2012). Evidence for a vertebrate origin of Smad3 rather than Smad2, and for Smad7 rather than Smad6 derives from analyses of conservation and expression in fly wings (supplementary table S8, Supplementary Material online; Marquez et al. 2001). Thus, in the vertebrate lineage Nedd4L was freed from the responsibility of ubiquitylating Smad4 by TIF1-γ/TRIM33 at the same time that duplications were creating new TGF-β pathways. Nedd4L then adopted the novel function of regulating the vertebrate-specific signal transducers Smad3 and Smad7.

Multi-Step Model of New Gene Evolution and the Dynamic Nature of Developmental Networks

Taken together the results suggest an expansion of the classic model for the origin of new genes and their acquisition of novel functions based on gene duplication. What is necessary is the inclusion of a potential intermediate step in the process. In this step, new genes resulting from duplication do not immediately assume a novel function themselves, but instead they assume the function of an existing gene. This substitution then allows the gene whose function was replaced to acquire a novel function.

Studies in *Drosophila* revealed that the rapid incorporation of new genes into existing genetic networks underlies their requirement for fertility and foraging behavior (Chen et al. 2013; Long et al. 2013). Thus, a prediction is that the incorporation of new genes into developmental networks underlies their requirement for viability. Our data that the new gene TIF1-γ/TRIM33 replaced the function of the existing gene Nedd4L in the vertebrate dorsal–ventral patterning network validate this prediction. The replacement of the Nedd4 HECT domain ubiquitin ligase by the TIF1-γ/TRIM33 RING domain ligase as an antagonist of the vertebrate BMP gradient is consistent with a study of the cave crustacean *Asellus aquaticus* (Protas et al. 2011). That study also showed that developmental phenotypes (in their case eye loss) can be achieved by multiple underlying genetic mechanisms.

As was demonstrated for the Hippo signaling network (Bossuyt et al. 2014), our data indicate that the architecture of the vertebrate dorsal–ventral patterning network was not simply conserved since the divergence from their common ancestor with flies. Instead these two networks were impacted by the acquisition of new functions by existing genes or by the incorporation of new genes after divergence from each other. Thus, the vertebrate developmental program contains highly conserved features such as *Hox* genes and dynamic features such as Hippo signaling and the dorsal–ventral patterning network.

In summary, our data extend our understanding of developmental evolution and the architecture of two developmental networks. For developmental evolution, the nonconservation of Bonus and TIF1-γ/TRIM33 functions in the conserved Dpp/BMP dorsal–ventral patterning pathway reveals that new genes may displace an existing gene, allowing the displaced gene to assume a novel function. For developmental networks, our data reveal that Bonus is a common signal transducer in the Toll and Dpp pathways whose function is likely mediated by distinct mechanisms. We conclude that the architecture of the Dpp/BMP dorsal–ventral patterning network continued to evolve in the vertebrate lineage, after the separation from arthropods, via the incorporation of new genes.

Materials and Methods

Identification of Human TIF1-δ/TRIM66 Isoform1

Alignment of human and mouse TIF1-δ/TPIM66 isoforms showed that the human initiator methionine is homologous to the methionine at position103 in mouse isoform1 and to the initiator methionine of mouse isoforms2 and 3. TBLASTN was employed to query the human RefSeq Genomic database with the N-terminal region of mouse isoform1. This identified two regions in the human genome upstream of the current TIF1-δ/TRIM66 start site that displayed significant similarity when translated. One region is 20-kb distant and the other is immediately adjacent to the current initiator methionine. The distantly upstream genomic region contains an in-frame methionine that was identified as a potential new start codon. However, there are stop codons in all three frames roughly 100–120 amino acids downstream of this new initiator methionine. Further analysis identified potential splice sites deleting the stop codons and allowing an open-reading frame containing the new initiator methionine and a RING domain to connect in-frame with the immediately upstream region. The immediately upstream region then continues in-frame into the current TIF1-δ/TRIM66 sequence. TBLASTN revealed that sequences encoding peptides with 98% identity to the 5′-extension of human TIF1-δ/TRIM66 are present in the *Pan troglodytes* chromosome 11 genomic scaffold. TBLASTN with the proposed upstream extension of human Tif1-δ/TRIM66 was utilized to query the human expressed sequence tag (EST) database. This analysis identified an EST (TESTI4024751) containing both the donor and acceptor sites confirming their existence. However, the EST does not directly join the two splice sites together. This suggests

human TIF1-δ/TRIM66 isoform3 contains three additional exons between the start of isoform1 and the current TIF1-δ/TRIM66. GenBank recently added a new prediction for a HsTIF1-δ/TRIM66 isoform that contains a nearly identical 5′-extension (GI 530396083 and Protein XP_005253327.1).

Phylogenetics

An alignment of 47 sequences (supplementary table S1, Supplementary Material online) was created with default settings in the Clustal Omega server at the EMBL-EBI website (www.ebi.ac.uk/Tools/msa/clustalo/) and visually inspected. Neighbor Joining and Maximum Likelihood trees were generated in MEGA5 (Tamura et al. 2011). For both methods, bootstrap consensus trees are inferred from 1,000 replicates and evolutionary distances computed using the Poisson correction method. Bootstrap values above 70 are considered statistically significant (Sitnikova 1996). Bayesian trees were created in MrBayes 3.2 (Ronquist et al. 2011). The prior amino acid model was set to Poisson (assumes equal stationary state frequencies and equal substitution rates; mrbayes.sourceforge.net/). The number of generations was set to 100,000 with a sample frequency of 100 and burn-in of 0.25. Posterior probabilities above 0.95 are considered significant. Other parameters were set to default.

Domains and Comparisons

Known structural or functional domains were predicted via SMART at EMBL (http://smart.embl-heidelberg.de/). The *E* value for a given region represents the number of sequences with a score greater than, or equal to, the score of the query sequence that can be expected absolutely by chance as calculated by Hidden Markov Models. Pairwise alignments of individual domains were generated with EMBOSS Needle at EMBL-EBI (http://www.ebi.ac.uk/Tools/psa/), a program employing the Needleman–Wunsch algorithm to produce an optimal global alignment of two sequences. The score was determined using the Blosum62 matrix with a gap penalty of −10.

Mutants

Fly stocks are as described: $bonus^{S048706}$ and $bonus^{21B}$ (Beckstead et al. 2001); $bonus^{EY1763}$ (Bellen et al. 2004), dpp^{hr4}, and dpp^{hr27} (Spencer et al. 1982); faf^{B6} (Fischer-Vize et al. 1992), $hiw^{BG02015}$, and hiw^{EP1308} (Wan et al. 2000); $Medea^{15}$ and $Medea^{17}$ (Hudson et al. 1998); $nedd4^{DG05310}$ (Huet et al. 2002); $nedd4^{T119FS}$ (Sakata et al. 2004), sog^{y506} (Ferguson and Anderson 1992); $smurf^{KG07014}$ (Tyler et al. 2007); nos.Gal4:VP16-MVD1 (van Doren et al. 1998); and UASp.GFP-αTub84B (Grieder et al. 2000). $Toll^{r3}$, $Toll^{r4}$, and $Toll^{8}$ were originally known as $Toll^{r632}$, $Toll^{rm9/rm10}$, and $Toll^{10B}$, respectively (Anderson, Bokla, et al. 1985; Anderson, Jürgens, et al. 1985). $bonus^{21B}$ is a small deletion resulting from an imprecise excision of a P-element in the 5′-untranslated region of exon1. This deletion does not affect the promoter. It eliminates all but the first 12 nt of exon1 including the initiator methionine as well as the splice acceptor and 324 nt of intron1. However, low level expression of nearly full-length Bonus is visible on Westerns and in embryos (Beckstead et al. 2001). Within the remaining 12 nt of exon1 is a methionine that if connected to the splice donor at the 5′-end of exon2 would result in a protein missing only the coding portion of exon1 (roughly 5% of the protein). Such a protein would contain all of the functional domains of full-length Bonus. $bonus^{487}$ has a P element insertion in intron1 that acts as a strong loss of function allele. $bonus^{EY1763}$ has a P element insertion in the 5′-untranslated region of exon1 that acts as a weak loss of function allele (Bellen et al. 2004). $Toll^{r3}$ is recessive loss of function allele with moderate effect and no identifiable mutations (Anderson, Bokla, et al. 1985; Anderson, Jürgens, et al. 1985; Schneider et al. 1991). $Toll^{r4}$ is a recessive loss of function allele associated with modest haploinsufficiency with two missense mutations in the extracellular domain (Anderson, Bokla, et al. 1985; Anderson, Jürgens, et al. 1985; Schneider et al. 1991). Temperature sensitivity of $Toll^{r3}/Toll^{r4}$ is as described (Wang et al. 2005). $Toll^{8}$ is a dominant gain of function allele with a missense mutation in the extracellular domain (Anderson, Bokla, et al. 1985; Anderson, Jürgens, et al. 1985; Erdelyi and Szabad 1989; Schneider et al. 1991). Standard blue balancers and germline clone-related strains are described in Flybase (Marygold et al. 2013).

Genetics

Toll maternal effect mutations were analyzed in two ways. First, in embryos derived from matings of $Toll^{r4}/+$ or $Toll^{8}/+$ females with wild type males. Second, egg-lays containing temperature-sensitive, transheterozygous $Toll^{r3}/Toll^{r4}$ females were collected at the permissive temperature (18 °C) and maintained at that temperature through virgin collection. $Toll^{r3}/Toll^{r4}$ females were mated to wild type males at the restrictive temperature (25 °C) and embryos aged 4 h at that temperature before fixation. Germline clone bearing females were generated employing a FRT82B $bonus^{21B}$ chromosome (Beckstead et al. 2001). FRT82B arm-lacZ was employed as a control for germline clone induction as described (Chou and Perrimon 1996). In brief, germline clone bearing females were mated to $bonus^{21B}$ heterozygous males to assay $bonus^{21B}$ homozygous embryos and paternally rescued heterozygous embryos. Germline clone embryos containing a paternal $bonus^{21B}$ chromosome were identified via wild type Bonus antibody staining. The only difference from the published germline clone method was that heat shocks were employed on Day 8 (pupal ages 144–192 AEL) and Day 9 (168–216 AEL).

Embryos

Cuticle preparations, antibody staining, and RNA in situ hybridization were as described (Stinchfield et al. 2012). Primary antibodies were: Hindsight (DSHB-1G9), Dorsal (DSHB-7A4), lacZ (DSHB-401A and Organon Teknika), Bonus-GP37 (Beckstead et al. 2001), pSmad (Epitomics), and pH3 (Abcam). Primary antibodies were detected with Alexa Fluor 488, 546, or 633 goat α-rabbit, α-mouse, α-sheep, or α-guinea pig (Molecular Probes) or with VectaStain Elite (Vector Labs). eGFP and DAPI (Sigma) were visualized directly. Labeled Dpp-HI cDNAs were detected with α-DIG

according to Takaesu et al. (2008). Pixel intensity plots reflecting pMad expression were created from single channel images in ImageJ. A single perpendicular line was drawn at the midpoint of the embryonic A/P axis. Pixel intensity along the line was analyzed with Plot Profile and the pixel intensity values were imported into Excel and graphed.

Supplementary Material

Supplementary tables S1–S8 and figures S1–S14 are available at *Molecular Biology and Evolution* online (http://www.mbe.oxfordjournals.org/).

Acknowledgments

The authors thank the following: Estela Arciniega, Hugo Bellen, Ela Serpe, Osamu Shimmi, Nancy Tran, Bloomington Stock Center, and Iowa Hybridoma Bank. This work was supported by National Institute of Health grants to S.J.N. (HG002516 and NS072128). The authors declare no competing financial interests. S.J.N. designed research and wrote paper; R.G.W., J.C.Q., M.J.S., and S.J.N. performed research; R.G.W., J.C.Q., and S.J.N. analyzed data.

References

Agricola E, Randall R, Gaarenstroom T, Dupont S, Hill CS. 2011. Recruitment of TIF1-γ to chromatin via its PHD finger-bromodomain activates its ubiquitin ligase and transcriptional repressor activities. *Mol Cell.* 43:85–96.

Alarcón C, Zaromytidou A, Xi Q, Gao S, Yu J, Fujisawa S, Barlas A, Miller AN, Manova-Todorova K, Macias MJ, et al. 2009. Nuclear CDKs drive Smad activation and turnover in BMP and TGF-β pathways. *Cell* 139:757–769.

Almada A, Wu X, Kriz A, Burge C, Sharp PA. 2013. Promoter directionality is controlled by U1 snRNP and polyadenylation signals. *Nature* 499:360–366.

Anderson KV. 1998. Pinning down positional information: dorsal–ventral polarity in the *Drosophila* embryo. *Cell* 95:439–442.

Anderson KV, Bokla L, Nüsslein-Volhard C. 1985. Establishment of dorsal–ventral polarity in the *Drosophila* embryo: induction of polarity by *Toll*. *Cell* 42:791–798.

Anderson KV, Jürgens G, Nüsslein-Volhard C. 1985. Establishment of dorsal–ventral polarity in the *Drosophila* embryo: genetic studies of *Toll*. *Cell* 42:779–789.

Aragón E, Goerner N, Xi Q, Gomes T, Gao S, Massagué J, Macias M. 2012. Structural basis for the interactions of Smad7 with WW domains in TGF-β pathways. *Structure* 20:1726–1736.

Aragón E, Goerner N, Zaromytidou A, Xi Q, Escobedo A, Massagué J, Macias M. 2011. A Smad action turnover switch operated by WW domain readers of a phosphoserine code. *Genes Dev.* 25:1275–1288.

Beckstead R, Ner S, Hales K, Grigliatti T, Baker BS, Bellen H. 2005. Bonus, a *Drosophila* TIF1 homolog, is a chromatin-associated protein that acts as a modifier of position-effect variegation. *Genetics* 169:783–794.

Beckstead R, Ortiz J, Sanchez C, Prokopenko S, Chambon P, Losson R, Bellen H. 2001. Bonus, a *Drosophila* homolog of TIF1 proteins, interacts with nuclear receptors and can inhibit FTZ-F1-dependent transcription. *Mol Cell.* 7:753–765.

Bellen H, Levis R, Liao G, He Y, Carlson JW, Tsang G, Evans-Holm M, Hiesinger PR, Schulze KL, Rubin GM, et al. 2004. BDGP gene disruption project: transposon insertions associated with 40% of *Drosophila* genes. *Genetics* 167:761–781.

Bossuyt W, Chen C, Chen Q, Sudol M, McNeill H, Pan D, Kopp A, Halder G. 2014. An evolutionary shift in the regulation of the Hippo pathway between mice and flies. *Oncogene* 33:1218–1228.

Boudinot P, van der Aa L, Jouneau L, Du Pasquier L, Pontarotti P, Briolat V, Benmansour A, Levraud J. 2011. Origin and evolution of TRIM proteins: new insights from the complete TRIM repertoire of zebrafish and pufferfish. *PLoS One* 6:e22022.

Chen S, Krinsky B, Long M. 2013. New genes as drivers of phenotypic evolution. *Nat Rev Genet.* 14:645–660.

Chen S, Ni X, Krinsky B, Zhang Y, Vibranovski M, White KP, Long M. 2012. Reshaping of global gene expression networks and sex-biased gene expression by integration of a young gene. *EMBO J.* 31:2798–2809.

Chen S, Spletter M, Ni X, White KP, Luo L, Long M. 2012. Frequent recent origination of brain genes shaped the evolution of foraging behavior in *Drosophila*. *Cell Rep.* 1:118–132.

Chen S, Zhang Y, Long M. 2010. New genes in *Drosophila* quickly become essential. *Science* 330:1682–1685.

Chou T, Perrimon N. 1996. The autosomal FLP-DFS technique for generating germline mosaics in *Drosophila*. *Genetics* 144:1673–1679.

De Robertis EM. 2008. Evo-devo: variations on ancestral themes. *Cell* 132:185–195.

Deshaies R, Joazeiro C. 2009. Ring domain E3 ubiquitin ligases. *Ann Rev Biochem.* 78:399–434.

Drier E, Huang L, Steward R. 1999. Nuclear import of the *Drosophila* Rel protein Dorsal is regulated by phosphorylation. *Genes Dev.* 13:556–568.

Dupont S, Inui M, Newfeld S. 2012. Regulation of TGF-β signal transduction by mono- and deubiquitylation of Smads. *FEBS Lett.* 586:1913–1920.

Dupont S, Mamidi A, Cordenonsi M, Montagner M, Zacchigna L, Adorno M, Martello G, Stinchfield MJ, Soligo S, Morsut L, et al. 2009. FAM/USP9X a deubiquitinating enzyme in TGF-β signaling controls Smad4 monoubiquitination. *Cell* 136:123–135.

Dupont S, Zacchigna L, Cordenonsi M, Soligo S, Adorno M, Rugge M, Piccolo S. 2005. Germ-layer specification and control of cell growth by Ectodermin, a Smad4 ubiquitin ligase. *Cell* 121:87–99.

Erdelyi M, Szabad J. 1989. Isolation and characterization of dominant female sterile mutations of *Drosophila*. I. Mutations on the third chromosome. *Genetics* 122:111–127.

Ferguson EL, Anderson KV. 1992. Dpp acts as a morphogen to organize dorsal–ventral pattern in the *Drosophila* embryo. *Cell* 71:451–461.

Fischer-Vize J, Rubin G, Lehmann R. 1992. The *fat facets* gene is required for *Drosophila* eye and embryo development. *Development* 116:985–1000.

Gao S, Alarcón C, Sapkota G, Rahman S, Chen P, Goerner N, Macias M, Erdjument-Bromage H, Tempst P, Massagué J. 2009. Ubiquitin ligase Nedd4L targets activated Smad2/3 to limit TGF-β signaling. *Mol Cell.* 36:457–468.

Grieder N, de Cuevas M, Spradling A. 2000. The fusome organizes the microtubule network during oocyte differentiation in *Drosophila*. *Development* 127:4253–4264.

Haldane JBS. 1933. Part played by recurrent mutation in evolution. *Am Nat.* 67:5–19.

Holley S, Jackson P, Sasaim Y, Lum B, De Robertis EM, Hoffmann FM, Ferguson EL. 1995. A conserved system for dorsal–ventral patterning in insects and vertebrates involving *sog* and *chordin*. *Nature* 376:249–253.

Holley S, Neul J, Attisano L, Wrana J, Sasai Y, O'Connor MB, De Robertis EM, Ferguson EL. 1996. The *Xenopus* dorsalizing factor Noggin ventralizes *Drosophila* embryos by preventing Dpp from activating its receptor. *Cell* 86:607–617.

Hudson J, Podos S, Keith K, Simpson S, Ferguson EL. 1998. The *Drosophila Medea* gene is required downstream of Dpp and encodes a functional homolog of human Smad4. *Development* 125:1407–1420.

Huet F, Lu J, Myrick K, Baugh L, Crosby M, Gelbart W. 2002. A deletion-generator compound element allows saturation analysis for genomewide phenotypic annotation. *Proc Natl Acad Sci U S A.* 99:9948–9953.

Ito H, Sato K, Koganezawa M, Ote M, Matsumoto K, Hama C, Yamamoto D. 2012. Fruitless recruits two antagonistic chromatin factors to establish single-neuron sexual dimorphism. *Cell* 149:1327–1338.

Kahlem P, Newfeld S. 2009. Informatics approaches to understanding TGF-β pathway regulation. *Development* 136:3729–3740.
Khetchoumian K, Teletin M, Mark M, Lerouge T, Cerviño M, Oulad-Abdelghani M, Chambon P, Losson R. 2004. TIF1-δ a novel HP1-interacting member of the TIF1 family expressed by elongating spermatids. *J Biol Chem.* 279:48329–48341.
Konikoff C, Wisotzkey R, Stinchfield M, Newfeld SJ. 2010. Distinct molecular evolutionary mechanisms underlie the functional diversification of the Wnt and TGF-β pathways. *J Mol Evol.* 70:303–312.
Le Douarin B, Nielsen A, Garnier J, Ichinose H, Jeanmougin F, Losson R, Chambon P. 1996. A possible involvement of TIF1-α and TIF1-β in the epigenetic control of transcription by nuclear receptors. *EMBO J.* 15:6701–6715.
Liang Y, Lin X, Liang M, Brunicardi F, ten Dijke P, Chen Z, Choi K, Feng XH. 2003. dSmurf selectively degrades Dpp-activated Mad and its overexpression disrupts imaginal disc development. *J Biol Chem.* 278: 26307–26310.
Long M, VanKuren N, Chen S, Vibranovski M. 2013. New gene evolution: little did we know. *Annu Rev Genet.* 47:325–351.
Marin I. 2012. Origin and diversification of TRIM ubiquitin ligases. *PLoS One* 7:e50030.
Marquez R, Singer M, Takaesu N, Waldrip W, Kraytsberg Y, Newfeld SJ. 2001. Transgenic analysis of the Smad family of TGF-β signal transducers suggests new roles and new interactions between family members. *Genetics* 157:1639–1648.
Marygold S, Leyland P, Seal R, Goodman J, Thurmond J, Strelets V, Wilson R, FlyBase Consortium. 2013. FlyBase: improvements to the bibliography. *Nucleic Acids Res.* 41:D751–D757.
McCabe B, Hom S, Aberle H, Fetter R, Marques G, Haerry T, Wan H, O'Connor MB, Goodman CS, Haghighi AP. 2004. Highwire regulates presynaptic BMP signaling essential for synaptic growth. *Neuron* 41: 891–905.
Morsut L, Yan K, Enzo E, Aragona M, Soligo SM, Wendling O, Mark M, Khetchoumian K, Bressan G, Chambon P, et al. 2010. Negative control of Smad activity by Ecto/Tif1-γ patterns the mammalian embryo. *Development* 137:2571–2578.
Muller HJ. 1936. Bar duplication. *Science* 83:528–530.
Newfeld SJ, Wisotzkey R, Kumar S. 1999. Molecular evolution of a developmental pathway: phylogenetic analyses of TGF-β family ligands, receptors and Smad signal transducers. *Genetics* 152:783–795.
Nielsen A, Ortiz J, You J, Oulad-Abdelghani M, Khechumian R, Gansmuller A, Chambon P, Losson R. 1999. Interaction with HP1 family members and histone deacetylation are differentially involved in transcriptional silencing by members of the TIF1 family. *EMBO J.* 18:6385–6395.
Nomura T, Tanikawa J, Akimaru H, Kanei-Ishii C, Ichikawa-Iwata E, Khan M, Ito H, Ishii S. 2004. Oncogenic activation of c-Myb correlates with a loss of negative regulation by TIF1-β and Ski. *J Biol Chem.* 279: 16715–16726.
O'Connor MB, Umulis D, Othmer H, Blair S. 2006. Shaping BMP morphogen gradients in the *Drosophila* embryo and pupal wing. *Development* 133:183–193.
Podos S, Hanson K, Wang Y, Ferguson EL. 2001. The dSmurf ubiquitin ligase restricts BMP signaling spatially and temporally during *Drosophila* embryogenesis. *Dev Cell.* 1:567–578.
Pritchard D, Schubiger G. 1996. Activation of transcription in *Drosophila* embryos is a gradual process mediated by the nucleocytoplasmic ratio. *Genes Dev.* 10:1131–1142.
Protas M, Trontelj P, Patel NH. 2011. Genetic basis of eye and pigment loss in the cave crustacean *Asellus aquaticus*. *Proc Natl Acad Sci U S A.* 108:5702–5707.
Ragsdale E, Müller M, Rödelsperger C, Sommer RJ. 2013. A developmental switch coupled to the evolution of plasticity acts through a sulfatase. *Cell* 155:922–933.
Ray R, Arora K, Nusslein-Volhard C, Gelbart W. 1991. The control of cell fate along the dorsal–ventral axis of the *Drosophila* embryo. *Development* 113:35–54.
Ronquist F, Teslenko M, vanderMark P, Ayres D, Darling A, Hohna S, Larget B, Liu L, Suchard M, Huelsenbeck J. 2011. MrBayes3.2: efficient phylogenetic inference and model choice across a large model space. *Syst Biol.* 61:539–542.
Ross B, Rosin L, Thomae A, Hiatt M, Vermaak D, de la Cruz A, Imhof A, Mellone B, Malik HS. 2013. Stepwise evolution of essential centromere function in a *Drosophila* neogene. *Science* 340: 1211–1214.
Roth S, Stein D, Nusslein-Volhard C. 1989. A gradient of nuclear localization of Dorsal determines dorsoventral pattern in the *Drosophila* embryo. *Cell* 59:1189–1202.
Sakata T, Sakaguchi H, Tsuda L, Higashitani A, Aigaki T, Matsuno K, Hayashi S. 2004. *Drosophila* Nedd4 regulates endocytosis of Notch and suppresses its ligand-independent activation. *Curr Biol.* 14: 2228–2236.
Sardiello M, Cairo S, Fontanella B, Ballabio A, Meroni G. 2008. Genomic analysis of the TRIM family reveals two groups with distinct evolutionary properties. *BMC Evol Biol.* 8:225.
Schneider D, Hudson K, Lin T, Anderson KV. 1991. Dominant and recessive mutations define functional domains of Toll, a transmembrane protein required for dorsal–ventral polarity in the *Drosophila* embryo. *Genes Dev.* 5:797–807.
Shimmi O, Umulis D, Othmer H, O'Connor MB. 2005. Facilitated transport of Dpp/Scw by Sog/Tsg leads to robust patterning of the *Drosophila* blastoderm embryo. *Cell* 120:873–886.
Sitnikova T. 1996. Bootstrap method of interior-branch test for phylogenetic trees. *Mol Biol Evol.* 13:605–611.
Spencer F, Hoffmann FM, Gelbart W. 1982. *Decapentaplegic*: a gene complex affecting morphogenesis in *Drosophila*. *Cell* 28:451–461.
Steward R. 1989. Relocalization of the Dorsal protein from the cytoplasm to the nucleus correlates with its function. *Cell* 59:1179–1188.
Stinchfield M, Takaesu NT, Quijano JC, Castillo A, Tiusanen N, Shimmi O, Enzo E, Dupont S, Piccolo S, Newfeld SJ. 2012. Fat facets deubiquitylation of Medea/Smad4 modulates interpretation of a Dpp morphogen gradient. *Development* 139:2721–2729.
Tadros W, Goldman A, Babak T, Menzies F, Vardy L, Orr-Weaver T, Hughes T, Westwood J, Smibert C, Lipshitz H. 2007. Smaug is a regulator of maternal mRNA destabilization and its translation is activated by Pangu. *Dev Cell.* 12:143–155.
Takaesu NT, Bulanin D, Johnson A, Orenic T, Newfeld SJ. 2008. A combinatorial enhancer recognized by Mad, TCF and Brinker first activates then represses *dpp* expression in the posterior spiracles of *Drosophila*. *Dev Biol.* 313:829–843.
Tamura K, Peterson D, Peterson N, Stecher G, Nei M, Kumar S. 2011. MEGA5: molecular evolutionary genetics analysis using maximum likelihood, evolutionary distance and maximum parsimony methods. *Mol Biol Evol.* 28:2731–2739.
Tyler D, Li W, Zhuo N, Pellock B, Baker NE. 2007. Genes affecting cell competition in *Drosophila*. *Genetics* 175:643–657.
van Doren M, Williamson A, Lehmann R. 1998. Regulation of zygotic gene expression in *Drosophila* primordial germ cells. *Curr Biol.* 8: 243–246.
Wan H, DiAntonio A, Fetter R, Bergstrom K, Strauss R, Goodman CS. 2000. Highwire regulates synaptic growth in *Drosophila*. *Neuron* 26: 313–329.
Wang J, Tao Y, Reim I, Gajewski K, Frasch M, Schulz R. 2005. Expression, regulation and requirement of Toll in dorsal vessel formation in *Drosophila*. *Mol Cell Biol.* 25:4200–4210.
Whalen A, Steward R. 1993. Dissociation of Dorsal–Cactus complex and phosphorylation of Dorsal protein correlates with nuclear localization of Dorsal. *J Cell Biol.* 123:523–534.
Wharton K, Ray R, Gelbart W. 1993. An activity gradient of *dpp* is necessary for the specification of dorsal pattern in the *Drosophila* embryo. *Development* 117:807–822.
Wisotzkey R, Konikoff C, Newfeld SJ. 2012. Hippo pathway phylogenetics predicts monoubiquitylation of Salvador and Merlin/Nf2. *PLoS One* 7:e51599.
Wolpert L. 1969. Positional information and the spatial pattern of cellular differentiation. *J Theor Biol.* 25:1–47.
Wu X, Sharp PA. 2013. Divergent transcription: a driving force for new gene origination? *Cell* 155:990–996.

Eight Supplemental Tables

Table S1. Accession numbers.

Symbol	GI number	Protein number	Species[a]
Ac LOC101846096	524907846	XP_005109034	Aplysia californica
Bf BRAFLDRAFT_240325	26081752	XP_002603636	Branchiostoma floridae
Bf BRAFLDRAFT_85511	26082794	XP_002608924	Branchiostoma floridae
Ce NCL-1	17554338	NP_498684.1	Caenorhabditis elegans
Ce NHL-2	17553200	NP_498026.1	Caenorhabditis elegans
Ci_zf(bbox/ring)-1	19308307	NP_001122371	Ciona intestinalis
Ci_zf(bbox/ring/phd)-1	11834420	NP_001071923	Ciona intestinalis
Ct CAPTEDRAFT_102254	44372503	ELU12781.1	Capitella teleta
Ct CAPTEDRAFT_90967	44369524	ELT96190.1	Capitella teleta
Dm Bonus	24648457	NP_524724.2	Drosophila melanogaster
Dm BRAT	17136846	NP_476945.1	Drosophila melanogaster
Dm MeiP26	21355671	NP_652022.1	Drosophila melanogaster
Dr TIF1-δ/TRIM66	52848502	XP_005166454	Danio rerio
Dr TIF1-α/TRIM24	67514537	NP_001002870	Danio rerio
Dr TIF1-γ/TRIM33	34730025	NP_001002871	Danio rerio
Dr TRIM71	32667466	XP_690252.5	Danio rerio
Gg TIF1-α/TRIM24	51315978	XP_416340.4	Gallus gallus
Gg TIF1-β/TRIM28	51323955	XP_428095.4	Gallus gallus
Gg TIF1-δ/TRIM66	51318634	XP_004941449	Gallus gallus
Gg TIF1-γ/TRIM33	51322520	XP_418009.4	Gallus gallus
Gg TRIM71	16783040	NP_001032352	Gallus gallus
Hr HELRODRAFT_130735	55569546	ESN98699.1	Helobdella robusta
Hs TIF1-α/TRIM24	47419911	NP_056989.2	Homo sapiens
Hs TIF1-β/TRIM28	5032179	NP_005753.1	Homo sapiens
Hs TIF1-δ*/TRIM66	20997709[b]	NP_055633[b]	Homo sapiens
Hs TIF1-γ TRIM33	74027249	NP_056990.3	Homo sapiens
Hs TRIM37	52487176	NP_001005207	Homo sapiens
Hs TRIM71	84993742	NP_001034200	Homo sapiens
Mm TIF1-α/TRIM24	94420998	NP_659542.3	Mus musculus
Mm TIF1-β/TRIM28	17029584	NP_035718.2	Mus musculus
Mm TIF1-δ/TRIM66	45861756	AAS78676.1	Mus musculus
Mm TIF1-γ/TRIM33	56404945	Q99PP7.2	Mus musculus
Mm TRIM71	10994830	NP_001035968	Mus musculus
Sk LOC100367035	29124261	XP_002741201	Saccoglossus kowalevskii
Sk LOC100372618	29123009	XP_002735005	Saccoglossus kowalevskii
Sp LOC580275	39035004	XP_785438.3	Strongylocentrotus purpuratus
Tr LOC101061951	41090836	XP_003967661	Takifugu rubripes
Tr LOC101064561	41091315	XP_003970052	Takifugu rubripes
Tr LOC101073124	41089906	XP_003963016	Takifugu rubripes
Tr LOC101076050	41091117	XP_003969064	Takifugu rubripes
Tr LOC101078035	41091901	XP_003972979	Takifugu rubripes
Xt TIF1-α/TRIM24	18923024	NP_001121448	Xenopus tropicalis
Xt TIF1-β/TRIM28	30161644	XP_002937648	Xenopus tropicalis
Xt TIF1-δ/TRIM66	51283299	XP_002942909	Xenopus tropicalis
Xt TIF1-γ/TRIM33	11860117	NP_001073032	Xenopus tropicalis
Xt TRIM71	42593626	F6QEU4.1	Xenopus tropicalis

a. Taxonomy and nomenclature. Vertebrates: Human Hs, Mouse Mm, Checken Gg, Frog Xt, Sebrafish Dr and PufferfishTr. Vertebrate closest relatives: Cephalochordate Bf, Hemichordate Sk, Urochordate Ci and Echinoderm Sp. Lophotrocozoans: Annelid Ct, Leech Hr and Mollusc Ac. Arthropod: Dm. Nematode: Ce. In the TRIM family naming is highly variable with the mouse names utilizing the TIF1 prefix and human names employing TRIM. We consistently apply both names while excluding unique names such as Ectodermin for TIF1-γ/TRIM33.

b. The 5' extended HsTIF1-δ*/TRIM66 was employed to generate the alignment underlying all trees. The existing prediction for HsTIF1-δ/TRIM66 does not contain a RING domain but the extended isoform we identified from genomic sequence conforms to the RING domain bearing mouse TIF1-δ/TRIM66 isoform1 (see Material and Methods and Figs. S1-4). Note the most recent release of Genbank contains a new prediction for a HsTIF1-δ/TRIM66 isoform that contains a nearly identical 5' extension (GI 530396083 and Protein XP_005253327.1).

Table S2. Location and probability of known domains in the TRIM family.

Domain Name	Start	End	E-value
Bonus			
RING	83	130	0.00121
low complexity	152	167	0.00121
BBOX	173	220	2.91E-06
BBOX	235	276	1.84E-08
BBC	283	409	2.15E-40
low complexity	448	491	2.15E-40
low complexity	583	605	2.15E-40
low complexity	612	627	2.15E-40
low complexity	650	669	2.15E-40
low complexity	777	794	2.15E-40
low complexity	810	824	2.15E-40
PHD	899	944	8.18E-10
BROMO	964	1071	7.17E-18
HsTIF1-β/TRIM28			
RING	65	120	1.58E-07
BBOX	148	195	2.97E-12
BBOX	204	245	1.11E-11
BBC	252	378	1.98E-39
low complexity	419	431	1.98E-39
low complexity	525	551	1.98E-39
PHD	627	670	2.16E-09
BROMO	697	801	1.34E-08
HsTIF1-α/TRIM24			
RING	76	130	6.00E-08
BBOX	158	205	6.27E-11
BBOX	218	259	2.22E-11
BBC	266	392	5.55E-43
low complexity	473	491	5.55E-43
low complexity	499	514	5.55E-43
low complexity	577	595	5.55E-43
low complexity	685	708	5.55E-43
low complexity	758	773	5.55E-43
PHD	828	871	3.15E-11
BROMO	901	1006	4.93E-39
low complexity	1017	1032	2.00E-17
HsTIF1-γ/TRIM33			
RING	125	184	2.61E-08
BBOX	212	259	1.24E-09
BBOX	271	312	1.54E-10
BBC	319	445	7.55E-45
low complexity	526	569	7.55E-45
low complexity	637	649	7.55E-45
low complexity	718	760	7.55E-45
low complexity	807	835	7.55E-45
low complexity	875	888	7.55E-45
PHD	889	932	4.15E-11
BROMO	959	1082	1.06E-29
Hs TIF1-δ*/TRIM66			
RING	33	86	0.9
BBOX	110	142	1.16
BBOX	170	211	0.0238
BBC	218	344	2.80E-39
PHD	1082	1125	1.35E-10
BROMO	1153	1259	3.58E-27

Table S3. Domain comparison between Bonus and TRIM proteins.

	HsTIF1-α/TRIM24	HsTIF1-β/TRIM28	HsTIF1-δ*/TRIM66	HsTIF1-γ/TRIM33
RING	Length: 54 Id: 21/54 (44%)[a] Sim: 25/54 (46%)[b] Gap: 19/54 (35%) Score: 94.0	Length: 56 Id: 17/56 (30%) Sim: 23/56 (41%) Gap: 08/56 (14%) Score: 78.5	Length: 58 Id: 18/58 (31%) Sim: 21/58 (36%) Gap: 14/58 (24%) Score: 52.5	Length: 60 Id: 21/60 (35%) Sim: 26/60 (43%) Gap: 12/60 (20%) Score: 89.0
BBOX	Length: 48 Id: 23/48 (48%) Sim: 36/48 (75%) Gap: 00/48 (00%) Score: 151.0	Length: 48 Id: 27/48 (56%) Sim: 38/48 (79%) Gap: 00/48 (00%) Score: 161.0	Length: 48 Id: 10/48 (21%) Sim: 08/48 (38%) Gap: 09/48 (19%) Score: 67.0	Length: 48 Id: 23/48 (48%) Sim: 34/48 (71%) Gap: 00/48 (00%) Score: 148.0
BBOX	Length: 42 Id: 24/42 (57%) Sim: 33/42 (79%) Gap: 00/42 (00%) Score: 155	Length: 42 Id: 23/42 (55%) Sim: 31/42 (74%) Gap: 00/42 (00%) Score: 145.0	Length: 42 Id: 20/42 (48%) Sim: 26/42 (62%) Gap: 00/42 (00%) Score: 119.0	Length: 42 Id: 23/42 (55%) Sim: 32/42 (76%) Gap: 00/42 (00%) Score: 150.5
BBC	Length: 130 Id: 29/130 (22%) Sim: 65/130 (50%) Gap: 08/130 (06%) Score: 113.0	Length: 128 Id: 31/128 (24%) Sim: 63/128 (49%) Gap: 02/128 (02%) Score: 119.0	Length: 127 Id: 25/127 (20%) Sim: 63/127 (50%) Gap: 00/127 (00%) Score: 133.0	Length: 131 Id: 30/131 (23%) Sim: 65/131 (50%) Gap: 06/131 (05%) Score: 103.0
PHD	Length: 46 Id: 26/46 (57%) Sim: 34/46 (74%) Gap: 02/46 (04%) Score: 173.5	Length: 46 Id: 19/46 (41%) Sim: 27/46 (59%) Gap: 02/46 (04%) Score: 115.5	Length: 46 Id: 28/46 (61%) Sim: 35/46 (76%) Gap: 02/46 (04%) Score: 175.5	Length: 46 Id: 26/46 (57%) Sim: 32/46 (70%) Gap: 02/46 (04%) Score: 169.5
BROMO	Length: 108 Id: 39/108 (36%) Sim: 58/108 (54%) Gap: 02/108 (02%) Score: 160.0	Length: 114 Id: 27/114 (24%) Sim: 41/114 (36%) Gap: 15/114 (13%) Score: 55.5	Length: 108 Id: 40/108 (37%) Sim: 54/108 (50%) Gap: 01/108 (01%) Score: 165.0	Length: 125 Id: 38/125 (30%) Sim: 61/125 (49%) Gap: 18/125 (14%) Score: 151.5
ALL	Length: 1251 Id: 316/1251 (25%) Sim: 488/1251 (39%) Gap: 319/1251 (26%) Score: 1000	Length: 1171 Id: 269/1171 (23%) Sim: 407/1171 (35%) Gap: 374/1171 (32%) Score: 725.0	Length: 1448 Id: 311/1448 (22%) Sim: 490/1448 (34%) Gap: 437/1448 (30%) Score: 718.0	Length: 1302 Id: 323/1302 (24%) Sim: 502/1302 (38%) Gap: 344/1302 (27%) Score: 972.5

a - red indicates the protein with the greatest percent identity to Bonus for that domain

b - blue indicates the protein with the greatest percent similarity to Bonus for that domain (identical amino acids plus conservative substitutions as defined biochemically)

Table S4. Cuticle defects in *bonus* zygotic mutants.

ventralized phenotypes	*bonus*^{487} / *bonus*^{21B}	*bonus*^{21B} / *bonus*^{EY1763}
wt (expect 100%)	82	86
herniated head	04	06
denticles extended	00	02
Filzkorper defects	10	04
partial U-shape	04	02

At least 50 cuticles were examined for each cross.

Table S5. *bonus* zygotic suppression of *sog*^{y506}.

paternal genotype	wt	*dpp*^{hr4} / +	*Medea*^{15}	*bonus*^{21B} / +	*faf*^{B6}/+
wt (expect 50%)	62	56	52	56	58
no denticles	30	12	08	16	18
denticles present/rescued	08	32	40	28	24

At least 50 cuticles were examined for each cross.

Table S6. Maternal heterozygosity for *nedd4* partially rescues *dpp*^{hr27} haploinsufficiency

maternal genotype	wt	*Medea*^{17}	*smurf*^{KG07014}/+	*nedd4*^{DG05310}/+	*nedd4*^{T119FS}/+	*hiw*^{BG02015}/*hiw*^{EP1308}
adult % expected	58[a]	01	84	80	78	61[b]

At least 200 adults were scored for each cross.

a. *dpp*^{hr27} haploinsufficiency is consistent with a previous report (Wharton et al. 1993).

b. This result is not statistically different from wild type.

Wharton K, Ray R, Gelbart W. 1993. An activity gradient of *dpp* is necessary for the specification of dorsal pattern in the *Drosophila* embryo. *Development* 117:807-822.

Table S7. Domain comparison between fly Nedd4 and two human Nedd4 proteins.

	HsNedd4	HsNedd4L
C2	Length: 108 Id: 62/108 (57%) Sim: 77/108 (71%) Gap: 09/108 (08%) Score: 294.5	Length: 106 Id: 63/106 (59%) Sim: 78/106 (74%) Gap: 04/106 (04%) Score: 312.5
WW	Length: 33 Id: 24/33 (73%) Sim: 25/33 (76%) Gap: 00/33 (00%) Score: 135.0	Length: 33 Id: 33/33 (100%) Sim: 33/33 (100%) Gap: 00/33 (00%) Score: 187.0
WW	Length: 33 Id: 14/33 (42%) Sim: 19/33 (58%) Gap: 00/33 (00%) Score: 82.0	Length: 33 Id: 33/33 (100%) Sim: 33/33 (100%) Gap: 00/33 (00%) Score: 189.0
WW	Length: 33 Id: 26/33 (79%) Sim: 29/33 (88%) Gap: 00/33 (00%) Score: 162.0	Length: 33 Id: 26/33 (79%) Sim: 29/33 (88%) Gap: 00/33 (00%) Score: 163.0
HECT	Length: 337 Id: 244/337 (72%) Sim: 282/337 (84%) Gap: 00/337 (00%) Score: 1351.0	Length: 337 Id: 238/337 (71%) Sim: 283/337 (84%) Gap: 00/337 (00%) Score: 1328.0
ALL	Length: 1043 Id: 488/1043 (47%) Sim: 606/1043 (58%) Gap: 179/1043 (17%) Score: 2299.5	Length: 1079 Id: 492/1079 (46%) Sim: 633/1079 (59%) Gap: 176/1079 (16%) Score: 2348.0

a - red as in Table S3

b - blue as in Table S3

Table S8. Domain comparison between fly Dad and two human Smad proteins.

	HsSmad6	HsSmad7
MH1	Length: 129 Id: 35/129 (27%) Sim: 53/129 (41%) Gap: 33/129 (26%) Score: 105.5	Length: 146 Id: 36/146 (25%) Sim: 53/146 (36%) Gap: 55/146 (38%) Score: 89.5
MH2	Length: 174 Id: 71/174 (41%) Sim: 86/174 (49%) Gap: 15/174 (09%) Score: 302.0	Length: 173 Id: 66/173 (38%) Sim: 94/173 (54%) Gap: 12/173 (07%) Score: 283.0
ALL	Length: 622 Id: 171/622 (28%) Sim: 227/622 (37%) Gap: 180/622 (29%) Score: 449.0	Length: 650 Id: 138/650 (21%) Sim: 193/650 (30%) Gap: 306/650 (47%) Score: 398.0

a - red as in Table S3 and S7

b - blue as in Table S3 and S7

Fourteen Supplemental Figures

```
MmTIF1-δ_isoform1     MSPGLPVSIPSQPHCSTDERVEALAPTCSMCGRDLQAEGSRLLPCQHLLCKDCYQ  55
MmTIF1-δ_isoform3     ---------------------------------------------------------
MmTIF1-δ_isoform2     ---------------------------------------------------------
HsTIF1-δ current      ---------------------------------------------------------

MmTIF1-δ_isoform1     GFMQELGHATRAYPGKLISCPGCQRVYLTRDVTEHIFLQCFSPVKPTMARNCSECKE 112
MmTIF1-δ_isoform2     ---------------------------------------------MARNCSECKE  10
MmTIF1-δ_isoform3     ---------------------------------------------MARNCSECKE  10
HsTIF1-δ current      ---------------------------------------------MARNCSECKE  10
```

Fig. S1. Alignment of human and mouse TIF1-δ/TRIM66 5' ends. Three experimentally identified isoforms of mouse TIF1-δ/TRIM66 are shown: isoform1 NP_001164383, isoform2 NP_862901 and isoform3 NP_001164384 (Khetchoumian et al., 2004). These are aligned with the current prediction for human TIF1-δ/TRIM66 (from the genomic scaffold of chromosome 11 corresponding to 11p15.4). Note that only mouse isoform1 contains the RING domain (Red) found in at least one isoform of all TIF1/TRIM family members and Bonus. Sequences identical in all TIF1-δ/TRIM66 isoforms are shown in green.

Khetchoumian K, Teletin M, Mark M, Lerouge T, Cerviño M, Oulad-Abdelghani M, Chambon P, Losson R. 2004. TIF1δ a novel HP1-interacting member of the TIF1 family expressed by elongating spermatids. *J Biol Chem*. 279:48329-48341.

A

```
     Score      Expect            Method             Identities   Positives   Gaps
68.2 bits(165) 2e-08  Compositional matrix adjust   33/65(51%)   44/65(67%)  2/65(3%)
Features: 19994bp at 5' side of TIF1-δ/TRIM66

Query  4         GLPVSIPSQPHCSTDERVEALAPTCSMCGRDLQAEGSRLLPCQHLLCKDCYQGFMQELGH  63
                 GLP++   Q HC    ++EA+  TCS+C +DL   GS LL CQHLL KDC+QG +QELG
Sbjct  8633537   GLPLA--GQKHCPKSGQMEAMVMTCSLCHQDLPGMGSHLLSCQHLLRKDCFQGLIQELGQ  8633364

Query  64        ATRAY  68
                   +A+
Sbjct  8633363   IAKAH  8633349
```

B

```
     Score     Expect            Method           Identities   Positives   Gaps
57.4 bits(137) 4e-05  Compositional matrix adjust   25/35(71%)   28/35(80%) 0/35(0%)
Features:  TIF1-δ/TRIM66

Query  71        KLISCPGCQRVYLTRDVTEHIFLQCFSPVKPTMAR  105
                 +LISCPGC+RVYLTRDVTEH FL C    +P MAR
Sbjct  8613451   ELISCPGCERVYLTRDVTEHFFLHCVPTEQPKMAR  8613347
```

Fig. S2. Identification of the RING domain in human TIF1-δ/TRIM66. Results of a TblastN query employing the N-terminal region of mouse TIF1-δ/TRIM66 isoform1 against the human RefSeq Genomic database. A) Region of significant similarity is identified roughly 20kb upstream of the current translation start codon. B) Region of significant similarity is identified immediately upstream and in-frame with the current translation start codon (underlined M).

A

```
MmTIF1-δ isoform1     -----MSPGLPVSIPSQPHCSTDERVEALAPTCSMCGRDLQAEGSRLLPCQHLLCKDCYQ  55
MmTIF1-δ isoform3     ------------------------------------------------------------
MmTIF1-δ isoform2     ------------------------------------------------------------
HsTIF1-δ current       ------------------------------------------------------------
HsTIF1-δ_new          MAVDMGMSFMGLPLAGQKHCPKSGQMEAMVMTCSLCHQDLPGMGSHLLSCQHLLSKDCFQ  60


MmTIF1-δ isoform1     GFMQELGHATRAYP---GKLISCPGCQRVYLTRDVTEHIFLQCFSPVKPTMARNCSECKE 112
MmTIF1-δ isoform2     ------------------------------------------------MARNCSECKE  10
MmTIF1-δ isoform3     ------------------------------------------------MARNCSECKE  10
HsTIF1-δ current       ------------------------------------------------MARNCSECKE  10
HsTIF1-δ_new          GLIQELGQIAKAHETVADELISCPGCERVYLTRDVTEHFFLHCVPTEQPKMARNCSECKE 120
```

B

```
    Score      Expect          Method               Identities    Positives   Gaps
160 bits(404)  4e-37   Compositional matrix adjust  76/78(97%)   76/78(97%)   0/78(0%)
Features: 20167bp at 5' side of TIF1-δ/TRIM66

Query  1        MAVDMGMSFMGLPLAGQKHCPKSGQMEAMVMTCSLCHQDLPGMGSHLLSCQHLLSKDCFQ  60
                MAVDMGMSFMGLPLAGQKHCPKSGQMEAMVMTCSLCHQDLPGMG HLLSCQHLL KDCFQ
Sbjct  4346862  MAVDMGMSFMGLPLAGQKHCPKSGQMEAMVMTCSLCHQDLPGMGCHLLSCQHLLCKDCFQ  4346683

Query  61       GLIQELGQIAKAHETVAD  78
                GLIQELGQIAKAHETVAD
Sbjct  4346682  GLIQELGQIAKAHETVAD  4346629


     Score     Expect          Method               Identities    Positives   Gaps
79.3 bits(194) 1e-12  Compositional matrix adjust  35/35(100%)  35/35(100%) 0/35(0%)
Features: TIF1-δ/TRIM66

Query  79       ELISCPGCERVYLTRDVTEHFFLHCVPTEQPKMAR  113
                ELISCPGCERVYLTRDVTEHFFLHCVPTEQPKMAR
Sbjct  4326558  ELISCPGCERVYLTRDVTEHFFLHCVPTEQPKMAR  4326454
```

Fig. S3. Alignment of the new and current human 5' ends with mouse TIF1-δ/TRIM66. A) The new open reading frame created by connecting the distant upstream region, the immediately upstream region and the current sequence of human TIF1-δ/TRIM66 is shown. The presence of a well-defined RING domain in the new sequence that is 60% identical to the RING domain in mouse TIF1-δ/TRIM66 isoform1 is indicated (red). Sequences identical in all TIF1-δ/TRIM66 isoforms are shown in green. B) The 5' extension of the human TIF1-δ/TRIM66 open reading frame is 98% identical to sequences encoded by two regions of the *Pan troglodytes* chromosome 11 genomic scaffold (current translation start codon for human TIF1-δ/TRIM66 is the underlined M).

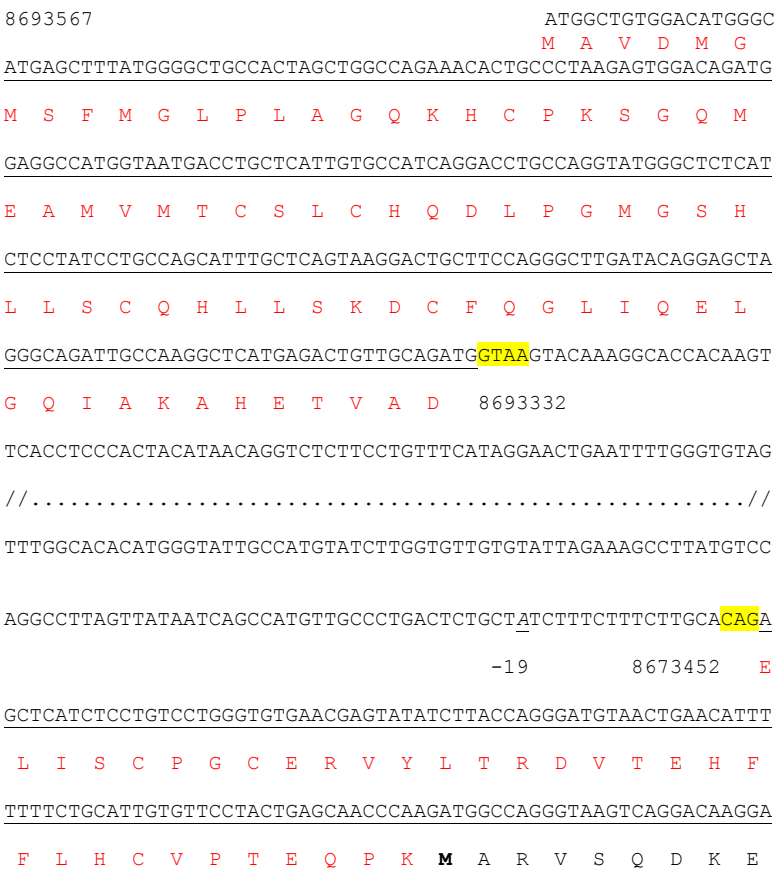

Fig. S4. Locations of new initiator methionine and splice sites for human TIF1-δ/TRIM66. Genomic sequence derived from GRCh37.p10 the primary assembly of human chromosome 11 is shown (NC_000011.9). Similarity to mouse TIF1-δ/TRIM66 isoform1 identifies the proposed new methionine at 8693567. An EST (TESTI4024751) identifies a splice donor site at 8693331 and a splice acceptor site at 8673452. The 5' and 3' ends of the intron are highlighted in yellow and the intervening 19880 nucleotides are shown as dots between pairs of forward slashes. A potential branch site at -19 from the splice acceptor site is underlined and italicized. The upstream extension of the current human TIF1-δ/TRIM66 open reading frame is in red with the corresponding nucleotide sequence underlined. The initiator methionine of the current human TIF1-δ/TRIM66 open reading frame is in bold.

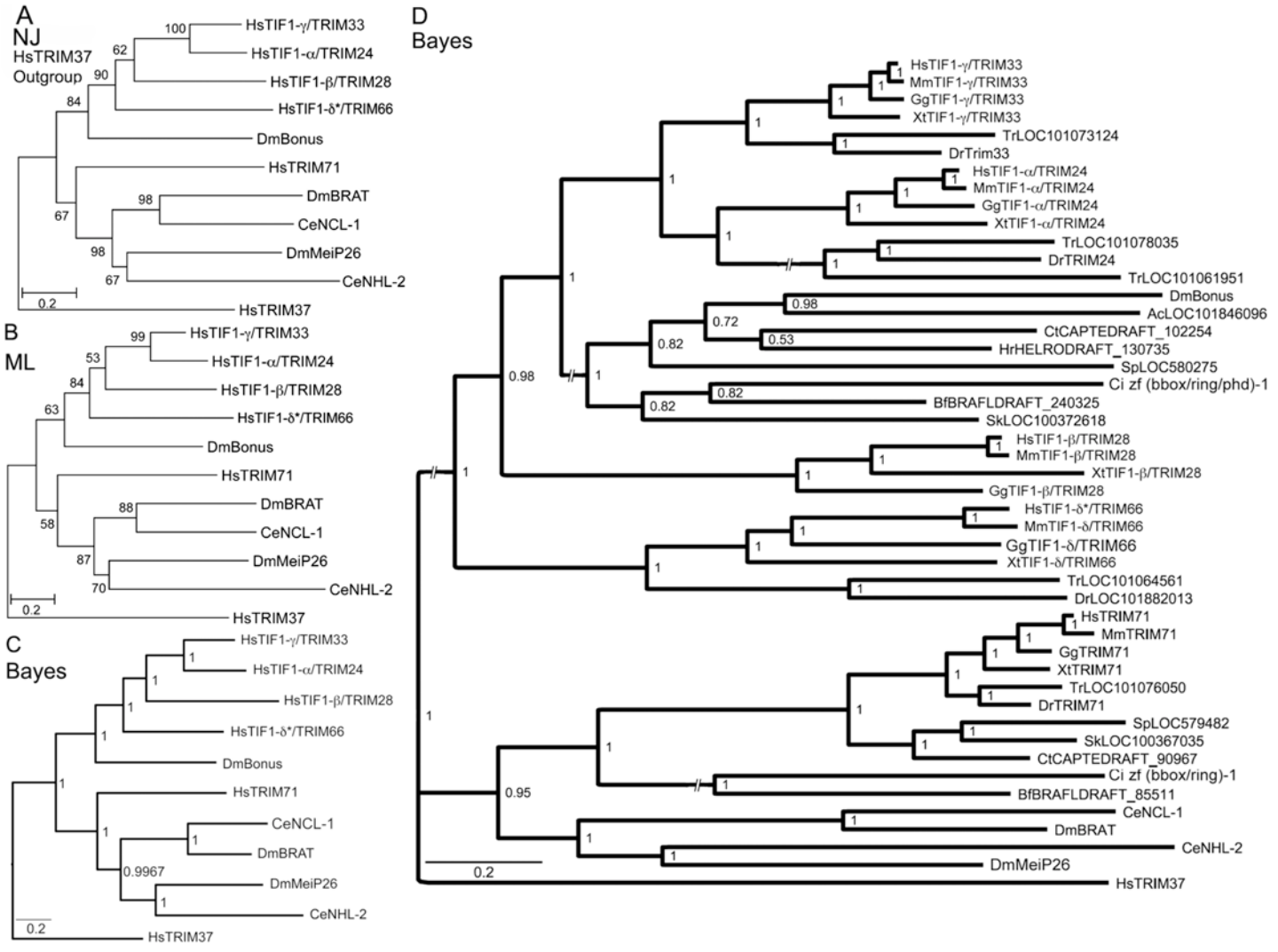
A
NJ
HsTRIM37
Outgroup
HsTIF1-γ/TRIM33
HsTIF1-α/TRIM24
HsTIF1-β/TRIM28
HsTIF1-δ*/TRIM66
DmBonus
HsTRIM71
DmBRAT
CeNCL-1
DmMeiP26
CeNHL-2
HsTRIM37
0.2
B
ML
HsTIF1-γ/TRIM33
HsTIF1-α/TRIM24
HsTIF1-β/TRIM28
HsTIF1-δ*/TRIM66
DmBonus
HsTRIM71
DmBRAT
CeNCL-1
DmMeiP26
CeNHL-2
HsTRIM37
0.2
C
Bayes
HsTIF1-γ/TRIM33
HsTIF1-α/TRIM24
HsTIF1-β/TRIM28
HsTIF1-δ*/TRIM66
DmBonus
HsTRIM71
CeNCL-1
DmBRAT
DmMeiP26
CeNHL-2
HsTRIM37
0.9967
0.2
D
Bayes
HsTIF1-γ/TRIM33
MmTIF1-γ/TRIM33
GgTIF1-γ/TRIM33
XtTIF1-γ/TRIM33
TrLOC101073124
DrTrim33
HsTIF1-α/TRIM24
MmTIF1-α/TRIM24
GgTIF1-α/TRIM24
XtTIF1-α/TRIM24
TrLOC101078035
DrTRIM24
TrLOC101061951
DmBonus
AcLOC101846096
CtCAPTEDRAFT_102254
HrHELRODRAFT_130735
SpLOC580275
Ci zf (bbox/ring/phd)-1
BfBRAFLDRAFT_240325
SkLOC100372618
HsTIF1-β/TRIM28
MmTIF1-β/TRIM28
XtTIF1-β/TRIM28
GgTIF1-β/TRIM28
HsTIF1-δ*/TRIM66
MmTIF1-δ/TRIM66
GgTIF1-δ/TRIM66
XtTIF1-δ/TRIM66
TrLOC101064561
DrLOC101882013
HsTRIM71
MmTRIM71
GgTRIM71
XtTRIM71
TrLOC101076050
DrTRIM71
SpLOC579482
SkLOC100367035
CtCAPTEDRAFT_90967
Ci zf (bbox/ring)-1
BfBRAFLDRAFT_85511
CeNCL-1
DmBRAT
CeNHL-2
DmMeiP26
HsTRIM37
0.98
0.72
0.53
0.82
0.82
0.95
0.2

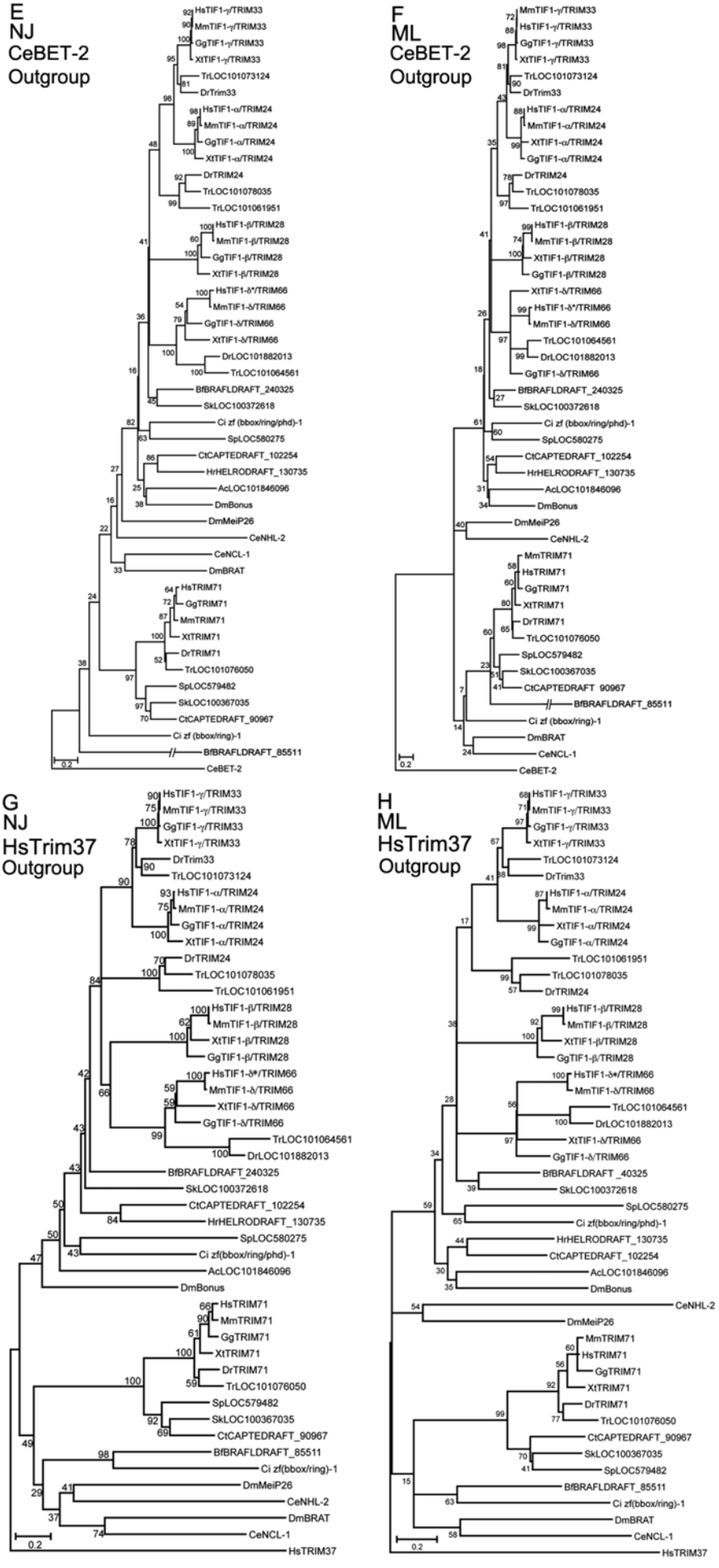
E
NJ
CeBET-2
Outgroup
HsTIF1-γ/TRIM33
MmTIF1-γ/TRIM33
GgTIF1-γ/TRIM33
XtTIF1-γ/TRIM33
TrLOC101073124
DrTrim33
HsTIF1-α/TRIM24
MmTIF1-α/TRIM24
GgTIF1-α/TRIM24
XtTIF1-α/TRIM24
DrTRIM24
TrLOC101078035
TrLOC101061951
HsTIF1-β/TRIM28
MmTIF1-β/TRIM28
GgTIF1-β/TRIM28
XtTIF1-β/TRIM28
HsTIF1-δ*/TRIM66
MmTIF1-δ/TRIM66
GgTIF1-δ/TRIM66
XtTIF1-δ/TRIM66
DrLOC101882013
TrLOC101064561
BfBRAFLDRAFT_240325
SkLOC100372618
Ci zf (bbox/ring/phd)-1
SpLOC580275
CtCAPTEDRAFT_102254
HrHELRODRAFT_130735
AcLOC101846096
DmBonus
DmMeiP26
CeNHL-2
CeNCL-1
DmBRAT
HsTRIM71
GgTRIM71
MmTRIM71
XtTRIM71
DrTRIM71
TrLOC101076050
SpLOC579482
SkLOC100367035
CtCAPTEDRAFT_90967
Ci zf (bbox/ring)-1
BfBRAFLDRAFT_85511
CeBET-2
0.2
F
ML
CeBET-2
Outgroup
MmTIF1-γ/TRIM33
HsTIF1-γ/TRIM33
GgTIF1-γ/TRIM33
XtTIF1-γ/TRIM33
TrLOC101073124
DrTrim33
HsTIF1-α/TRIM24
MmTIF1-α/TRIM24
XtTIF1-α/TRIM24
GgTIF1-α/TRIM24
DrTRIM24
TrLOC101078035
TrLOC101061951
HsTIF1-β/TRIM28
MmTIF1-β/TRIM28
XtTIF1-β/TRIM28
GgTIF1-β/TRIM28
XtTIF1-δ/TRIM66
HsTIF1-δ*/TRIM66
MmTIF1-δ/TRIM66
TrLOC101064561
DrLOC101882013
GgTIF1-δ/TRIM66
BfBRAFLDRAFT_240325
SkLOC100372618
Ci zf (bbox/ring/phd)-1
SpLOC580275
CtCAPTEDRAFT_102254
HrHELRODRAFT_130735
AcLOC101846096
DmBonus
DmMeiP26
CeNHL-2
MmTRIM71
HsTRIM71
GgTRIM71
XtTRIM71
DrTRIM71
TrLOC101076050
SpLOC579482
SkLOC100367035
CtCAPTEDRAFT_90967
BfBRAFLDRAFT_85511
Ci zf (bbox/ring)-1
DmBRAT
CeNCL-1
CeBET-2
0.2
G
NJ
HsTrim37
Outgroup
HsTIF1-γ/TRIM33
MmTIF1-γ/TRIM33
GgTIF1-γ/TRIM33
XtTIF1-γ/TRIM33
DrTrim33
TrLOC101073124
HsTIF1-α/TRIM24
MmTIF1-α/TRIM24
GgTIF1-α/TRIM24
XtTIF1-α/TRIM24
DrTRIM24
TrLOC101078035
TrLOC101061951
HsTIF1-β/TRIM28
MmTIF1-β/TRIM28
XtTIF1-β/TRIM28
GgTIF1-β/TRIM28
HsTIF1-δ*/TRIM66
MmTIF1-δ/TRIM66
XtTIF1-δ/TRIM66
GgTIF1-δ/TRIM66
TrLOC101064561
DrLOC101882013
BfBRAFLDRAFT_240325
SkLOC100372618
CtCAPTEDRAFT_102254
HrHELRODRAFT_130735
SpLOC580275
Ci zf(bbox/ring/phd)-1
AcLOC101846096
DmBonus
HsTRIM71
MmTRIM71
GgTRIM71
XtTRIM71
DrTRIM71
TrLOC101076050
SpLOC579482
SkLOC100367035
CtCAPTEDRAFT_90967
BfBRAFLDRAFT_85511
Ci zf(bbox/ring)-1
DmMeiP26
CeNHL-2
DmBRAT
CeNCL-1
HsTRIM37
0.2
H
ML
HsTrim37
Outgroup
HsTIF1-γ/TRIM33
MmTIF1-γ/TRIM33
GgTIF1-γ/TRIM33
XtTIF1-γ/TRIM33
TrLOC101073124
DrTrim33
HsTIF1-α/TRIM24
MmTIF1-α/TRIM24
XtTIF1-α/TRIM24
GgTIF1-α/TRIM24
TrLOC101061951
TrLOC101078035
DrTRIM24
HsTIF1-β/TRIM28
MmTIF1-β/TRIM28
XtTIF1-β/TRIM28
GgTIF1-β/TRIM28
HsTIF1-δ*/TRIM66
MmTIF1-δ/TRIM66
TrLOC101064561
DrLOC101882013
XtTIF1-δ/TRIM66
GgTIF1-δ/TRIM66
BfBRAFLDRAFT_40325
SkLOC100372618
SpLOC580275
Ci zf(bbox/ring/phd)-1
HrHELRODRAFT_130735
CtCAPTEDRAFT_102254
AcLOC101846096
DmBonus
CeNHL-2
DmMeiP26
MmTRIM71
HsTRIM71
GgTRIM71
XtTRIM71
DrTRIM71
TrLOC101076050
CtCAPTEDRAFT_90967
SkLOC100367035
SpLOC579482
BfBRAFLDRAFT_85511
Ci zf(bbox/ring)-1
DmBRAT
CeNCL-1
HsTRIM37
0.2

Fig. S5. Evolutionary relationships within the Bonus-Tif1-γ/TRIM33 subfamily are topologically consistent in multiple trees. A) Neighbor Joining (NJ), B) Maximum Likelihood (ML) and C) Bayesian trees of eleven human (Hs), fly (Dm) and nematode (Ce) TRIM family sequences from Table S1 related to Bonus. HsTRIM71 was chosen to anchor the non-Bonus fly and nematode sequences into a single subfamily. HsTRIM37 was chosen as the outgroup based Sardiello et al. (2008) indicating that HsTRIM37 did not cluster with any other human TRIM proteins. The alignment contained 517 informative positions. A scale bar showing amino acid substitutions per site is present. Bootstrap values (NJ tree and ML tree) above 40% or posterior probabilities above 0.5 (Bayesian tree) are shown. Bootstrap values above 70% and posterior probabilities above 0.95 are considered statistically significant. Each tree contains the same two distinct subfamilies. Within one subfamily Bonus is consistently the most distant sequence, either TIF1-β/TRIM28 or TIF1-δ/TRIM61 are the oldest vertebrate and TIF1-γ/TRIM33 is the youngest vertebrate sequence. D) Expanded Bayesian tree containing all 47 sequences in Table S1 derived from an alignment with 154 informative positions. The same two statistically supported subfamilies are visible. The topology of the Bonus-TIF1-γ/TRIM33 subfamily shows a slightly different topology than the other trees with Bonus midway between the four vertebrate sequences rather than as an outlier. E, F) Expanded NJ and ML trees employing CeBET-2 as an outgroup derived from an alignment with 173 informative positions and displaying all bootstrap values. G,H) Expanded NJ and ML trees employing HsTRIM37 as an outgroup derived from an alignment with 154 informative positions and displaying all bootstrap values. Each of the four large trees contains the same two distinct subfamilies with occasional non-significant outliers (e.g. CeNHL-2/DmMeiP26 in panel H). In the TIF1-γ/TRIM33 subfamily Bonus consistently maps as the most divergent sequence. Based on topology and branch lengths, either TIF1-β/TRIM28 or TIF1-δ/TRIM61 is the oldest and TIF1-γ/TRIM33 the youngest vertebrate sequence in this subfamily.

Sardiello M, Cairo S, Fontanella B, Ballabio A, Meroni G. 2008. Genomic analysis of the TRIM family reveals two groups with distinct evolutionary properties. *BMC Evol Biol*. 8:225

A

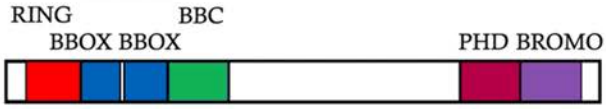

B

```
DmBonus          1   ------------------------MDMDLEQLKNDFLPLIAGIKQEQLDAVPTDALPQMS
HsTIF1-β/TRIM28  1   ------------------------------------------MAASAAAASAAAASAASG
HsTIF1-δ*/TRIM66 1   ------------------------------------------------MAVDMGMSFMG
HsTIF1-α/TRIM24  1   ------------------------------------------MEVAVEKAVAAAAAASAA
HsTIF1-γ/TRIM33  1   MAENKGGGEAESGGGGSGSAPVTAGAAGPAAQEAEPPLTAVLVEEEEEEGGRAGAEGGAA

DmBonus         37   TENTASGAPTTSSLSSSSLSLSNPCDSAEKRSESNSS------------------ASAKF
HsTIF1-β/TRIM28 19   SPGPGEGSAGGEKRSTAPSAAASASASAAASSPAGGG------------------PEALE
HsTIF1-δ*/TRIM66 12  LPLAGQKHCPKSGQMEA-----------------------------------------------
HsTIF1-α/TRIM24  19  AS--GGPSAAPSGENEAESRQGPDSER---GGEAAR----------------------LN
HsTIF1-γ/TRIM33  61  GEDDGGVAAASSGSAQAASSPAASVGTGVAGGAVSTPAPAPASAPAPGPSAGPPPGPPAS

DmBonus         79   TLFKGVYGAQLGGND--RPKLLECLHVAGAQGVSTKFSELDRSLP-------------P
HsTIF1-β/TRIM28 61   LLEHGGVGRERGRPER--EPRLLPCLHSAGSAGLGPAAPAAANSS---------------
HsTIF1-δ*/TRIM66 29  MVMTGGSLGHQDLPGMG---SHLLSPQHLLSKDGFQGLIQEIGQIAK--------------
HsTIF1-α/TRIM24  52  LLDTGAVGHQNIQSR---APKLLPCLHSFGQRGLPAPQRYEMLPAPMLGSAETPPPVPAP
HsTIF1-γ/TRIM33  121 LLDTGAVGQQSHQSRREAEPKLLPCLHSFGLRGLPEPERQESVPIP--------------

DmBonus         124  LIHCPVCDNASQQEFIVDNQFLIEQGTAGDSGDGVGLLGLHGEGQKSSAAASIQGSSCSD
HsTIF1-β/TRIM28 104  -----EDGGAAGDGTVVDCPVCKQQGFSKDIVENYFMRDSGSKAAHDAQDANGCTSCED
HsTIF1-δ*/TRIM66 72  -------AHETVADELISCPGCERVYLTRDVTEHFFLHCVPTEQPKMARN----CSECK-
HsTIF1-α/TRIM24  109 GSPVSGSSPFATTVGVIRCPVCSQEGAERHIIDNFFVKDTTEVPSSTVEKSNQVCTSCED
HsTIF1-γ/TRIM33  167 ----GESNGDIQLVGVIRCPVCRQEGRQIDLVDNYFVKDTSEAPSSSDEKSEQVCTSCED

DmBonus         184  GAVATSACVDCSEVICDSCVQAHQRLKITKDHTIKPKDEANNEQLAGAAGVDKLHMCQLH
HsTIF1-β/TRIM28 159  NAPATSPCVEGSEPLQETCMEAHQRVKYTKDHTVRSTGPAK------SRDGERTVVCNVH
HsTIF1-δ*/TRIM66 121 KRAAHILGTYCNRNLGSSGTSEHRHSPVPGGPFFPRAQKGSP--GVNGGPGDFTVYCPLH
HsTIF1-α/TRIM24  169 NAEANGPCVEGVEWLGKTCERAHQRVKFTKDHTVRQKEEVSP--EAVGVTSQRPVGCPEH
HsTIF1-γ/TRIM33  223 NASAVGPCVECGEWLGKTCIEAHQRVKFTKDHLIRRKEDVS---ESVGASGQRPVGCPVH

DmBonus         244  PQEKLSLFCETCDKLTCRDCQLSDHDDHKYKFAHEIATESRQALSDLVEELNYKRFLSS
HsTIF1-β/TRIM28 213  SHEPLVLFCPSCDTLTCRDCQLNAHKDHQYQFLEDAVRNQRKELAELLKKLGDKAATLQK
HsTIF1-δ*/TRIM66 179 TQEVLKLFCETCDMLTCHSCLVVEHKEHRCRHVEEVLQNQRMQLLRGVTQQAHKASSLQT
HsTIF1-α/TRIM24  227 KKEQLKLMCETCDRLTCRDCQLLEHKEHRYQFVEEAFQNQKEVLEKRLMEKTKYIKF
HsTIF1-γ/TRIM33  280 KQEQLKLFCETCDRLTCRDCQLLEHKEHRYQFVEEAFQNQHGALENLLAKLLEKLNYHHF

DmBonus         304  ATKVLDDRQQQLEHLKKKRDEIKRLTAMAMKVINTRNDKGKQLMREVEDCDSRLKVLEKK
HsTIF1-β/TRIM28 273  ITKEMRSSIRQVSHVEKMVQVQGKAIHQQKEIMKRGEVLNDAQKVTEGQQEILERQH
HsTIF1-δ*/TRIM66 239 IPKQIEDRIFEVKHQHEVEMQIKMAKSVLMNEMNKQRNGLEELEGITNSLKRKLEQQL
HsTIF1-α/TRIM24  287 IQNQIQNRIIEVNQNGKQVEGQIKVAIFTLMVEMNKRGKALHQLESLAKDMRMKLQQQQ
HsTIF1-γ/TRIM33  340 AITQLQNRIKEVNQTGKVEGQIKVAIFTLMNEMNKRGKSLQQLENVTKDLQMKLQQQQ

DmBonus         364  EETQLLSDMTHCADGMLNALEKGSDFALGSSKRGSLVRHLQKLKCQRADIPNPEIPVRIQ
HsTIF1-β/TRIM28 333  WHNTKLQGHQEHIRRGASWALESDNNTALLLSKGLIYFQLHHALEMIVDPV-EPHG-EMK
HsTIF1-δ*/TRIM66 299 GEIMVRNGQFEHVQNGIEWAVCSKGSVPFLSKELIVFQDQLLETSCNTD-PGSPWSIR
HsTIF1-α/TRIM24  347 GEHAGLSGQLEHVHHSKWAVSSGSSTALLPSKGLITFRLHLLLAARCDAS-PVTNNTIQ
HsTIF1-γ/TRIM33  400 EDITGLSSQVKHVHNGTWAVASGSSTALLPSKGLITFQLHILLAARCEPV-PAANGAIR

DmBonus         424  VQLNQVSDLQKVLSQLGIIIVDGKPYPPTPSP----------------------------
HsTIF1-β/TRIM28 391  EQWDLN-AWTKSAEAFGKIVAERP---------------------------------------
HsTIF1-δ*/TRIM66 358 ETWEPN-FWTKQLASLGCLLTEGGQMSRADAPAYGGLQGSSPFYQSHQSPVAQQEALS//
HsTIF1-α/TRIM24  406 EHCDPS-FWAQNIINLGSLVIEDKESQ-------------------------------------
HsTIF1-γ/TRIM33  459 EHCDPT-FWAKNVVNLGNLVIESK---------------------------------------

DmBonus         456  ----------------------NGTPQFQHPPRQPPSPNMAPPLRPGLPPGMPAGLSPNG
HsTIF1-β/TRIM28 414  ------------------------------GTNSTGPAP--------------------
HsTIF1-δ*/TRIM66 477 LPREKELACSPHPPKLLQPWLETQPPVEQESTSQRLGQQLTSQPVCIVPPQDVQQGAHAQ
HsTIF1-α/TRIM24  432 ------------------------PQMPKQNPVVEQNSQPPSGLSSNQLSKFPTQISLAQ
HsTIF1-γ/TRIM33  482 ------------------------PAPGYTPNVVVGQVPPG---TNHISKTPGQINLAQ

DmBonus         494  PPVNFGPQNGPPLYSNAAQQQFNNLSMSRSFPGDGSGKVRFGGMPPVGMQRHGQPHVSSS
HsTIF1-β/TRIM28 423  ------------------------------MAPPRAPGPLSKQGSGSSQP--------
HsTIF1-δ*/TRIM66 537 PTLQTPSIQVQFGHHQKLKLSHFQQQPQQQLPPPPPPLPHPPPPLPPPPQQPHPPLPPSQ
HsTIF1-α/TRIM24  468 LRLQHMQQQVMAQRQQ------VQRRPAPVG-LPNPRMQGPIQQPSISHQQPPRLINPQ
HsTIF1-γ/TRIM33  514 LRLQHMQQQVYAQKHQQLQQMRMQQPPAPVPTTTTTTQQHPRQAAPQMLQQQPPRLISVQ

DmBonus         554  THPQN-----------------------------------MDISLRGLLNNQAAQSPNAH
HsTIF1-β/TRIM28 443  ------------------------------------------------------------
HsTIF1-δ*/TRIM66 597 HLASSQHESPPGPACSQNMDIMHHKFELEEMQKDLELLLQAQQPSLQLSQTKSPQHLQQT
HsTIF1-α/TRIM24  521 NHSP-------------------------------------------KPNGPVLPPHPQQLR
HsTIF1-γ/TRIM33  574 TMQ-------------------------------------------RGNMNCGAPQAHQMR
```

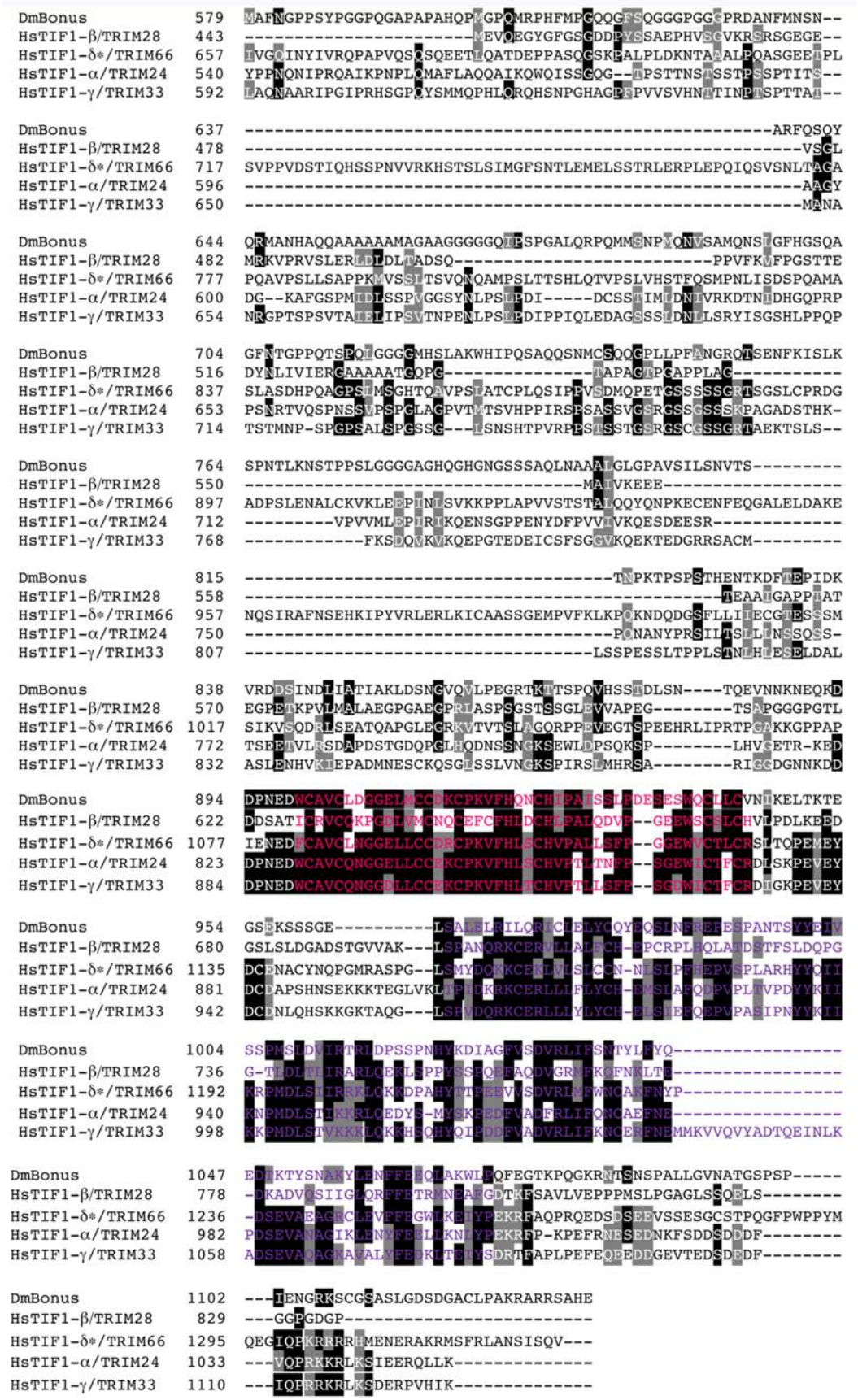
DmBonus 579
HsTIF1-β/TRIM28 443
HsTIF1-δ*/TRIM66 657
HsTIF1-α/TRIM24 540
HsTIF1-γ/TRIM33 592
DmBonus 637
HsTIF1-β/TRIM28 478
HsTIF1-δ*/TRIM66 717
HsTIF1-α/TRIM24 596
HsTIF1-γ/TRIM33 650
DmBonus 644
HsTIF1-β/TRIM28 482
HsTIF1-δ*/TRIM66 777
HsTIF1-α/TRIM24 600
HsTIF1-γ/TRIM33 654
DmBonus 704
HsTIF1-β/TRIM28 516
HsTIF1-δ*/TRIM66 837
HsTIF1-α/TRIM24 653
HsTIF1-γ/TRIM33 714
DmBonus 764
HsTIF1-β/TRIM28 550
HsTIF1-δ*/TRIM66 897
HsTIF1-α/TRIM24 712
HsTIF1-γ/TRIM33 768
DmBonus 815
HsTIF1-β/TRIM28 558
HsTIF1-δ*/TRIM66 957
HsTIF1-α/TRIM24 750
HsTIF1-γ/TRIM33 807
DmBonus 838
HsTIF1-β/TRIM28 570
HsTIF1-δ*/TRIM66 1017
HsTIF1-α/TRIM24 772
HsTIF1-γ/TRIM33 832
DmBonus 894
HsTIF1-β/TRIM28 622
HsTIF1-δ*/TRIM66 1077
HsTIF1-α/TRIM24 823
HsTIF1-γ/TRIM33 884
DmBonus 954
HsTIF1-β/TRIM28 680
HsTIF1-δ*/TRIM66 1135
HsTIF1-α/TRIM24 881
HsTIF1-γ/TRIM33 942
DmBonus 1004
HsTIF1-β/TRIM28 736
HsTIF1-δ*/TRIM66 1192
HsTIF1-α/TRIM24 940
HsTIF1-γ/TRIM33 998
DmBonus 1047
HsTIF1-β/TRIM28 778
HsTIF1-δ*/TRIM66 1236
HsTIF1-α/TRIM24 982
HsTIF1-γ/TRIM33 1058
DmBonus 1102
HsTIF1-β/TRIM28 829
HsTIF1-δ*/TRIM66 1295
HsTIF1-α/TRIM24 1033
HsTIF1-γ/TRIM33 1110

Fig. S6. Alignment of Bonus-TIF1-γ/TRIM33 subfamily proteins. A) Color-coded schematic of domains and their location in Bonus-TIF1-γ/TRIM33 subfamily proteins (RING - orange, BBOX - blue, BBC - green, PHD - crimson and BROMO - purple). B) Alignment of Bonus-TIF1-γ/TRIM33 subfamily proteins. The background of an amino acid is shaded if the residue is identical (black) or similar (grey) at that position in at least three sequences. The color of an amino acid indicates the location of a functional domain following the coordinates shown in Table S2 and the color-scheme above.

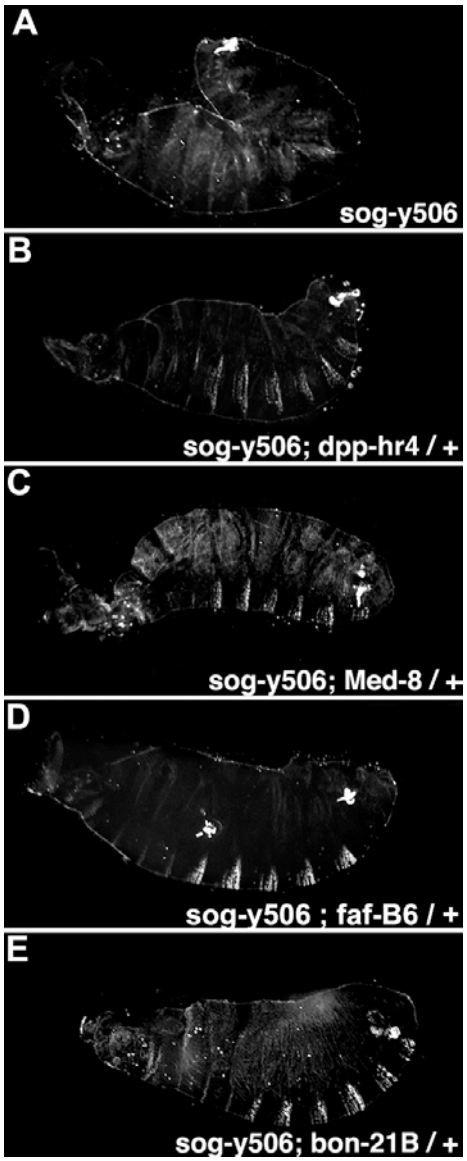

Fig. S7. *bonus* zygotic heterozygosity partially suppresses *sog* hemizygous mutant phenotypes. Cuticles in lateral view with anterior to the left and dorsal up. The maternally contributed allele is listed first. A) sog^{y506} hemizygous dorsalized cuticle containing no denticles, U-shaped body, herniated head and Filzkorper defects. B) sog^{y506} hemizygous and dpp^{hr4} heterozygous cuticle with head and Filzkorper defects but partially restored denticles and body shape. C) sog^{y506} hemizygous and $Medea^{8}$ heterozygous cuticle shows partial rescue. D) sog^{y506} hemizygous and $fat\ facets^{B6}$ heterozygous cuticle shows partial rescue. E) sog^{y506} hemizygous and $bonus^{21B}$ heterozygous cuticle shows partial rescue.

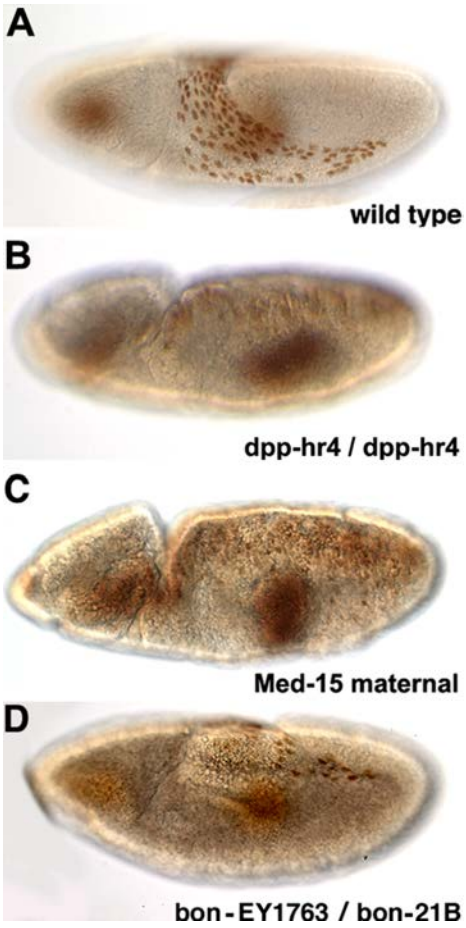

Fig. S8. Loss of Hindsight amnioserosa but not foregut or hindgut expression in *bonus* zygotic mutants. Stage 10 embryos in lateral view revealing Dpp-dependent Hindsight expression in amnioserosa cells. Dpp-independent Hindsight expression in the foregut and hindgut is visible below the plane of focus. The latter staining acts as an internal control and is observed in all genotypes. The maternally contributed allele is listed first. A) Wild type embryo. B) dpp^{hr4} homozygous ventralized embryo with a few scattered amnioserosa cells. C) Ventralized maternal $Medea^{15}$ embryo is similar to the dpp^{hr4} embryo with a few scattered amnioserosa cells. D) $bonus^{EY1763}/bonus^{21B}$ transheterozygous embryo with a reduced number of amnioserosa cells

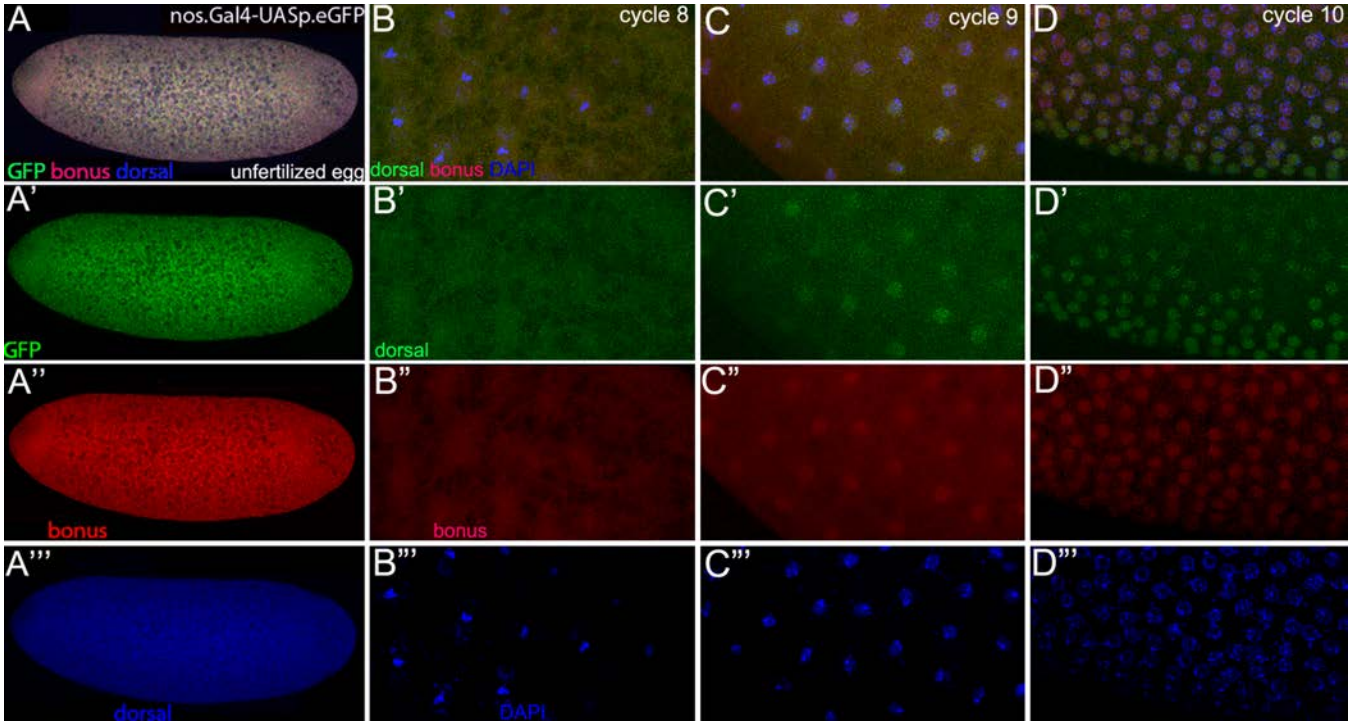

Fig. S9. Bonus and Dorsal are maternally loaded and cytoplasmic in eggs then translocate synchronously into nuclei at cycle 9. A) Unfertilized egg in lateral view from a female expressing UAS.eGFP under the control of the maternal driver nos.Gal4. Low magnification three-color and single channel images of eGFP (green), Bonus (red) and Dorsal (blue). All proteins are present and cytoplasmic. B-D) Wild type embryos in lateral view with ventral at the bottom. High magnification three color and single channel images of Dorsal (green), Bonus (red) and DAPI (blue). B) Cycle 8 embryo similar to Fig. 4A with uniformly cytoplasmic Dorsal and Bonus and uniformly nuclear DAPI. C) Cycle 9 embryo similar to Fig. 4B with cytoplasmic Dorsal toward the top (dorsal region) and a mix of nuclear and cytoplasmic Dorsal toward the bottom (ventral region) as well as a uniform mix of nuclear and cytoplasmic Bonus and uniformly nuclear DAPI. D) Cycle 10 embryo similar to Fig. 4C with cytoplasmic Dorsal toward the top (dorsal region) and nuclear Dorsal toward the bottom (ventral region) as well as uniformly nuclear Bonus and DAPI.

bonus exon1

A. nt16418861-16419766 Chromosome 3 sequence NT_033777.2

⮟ *bonus*^{21B} deleted from +12 to past exon1 splice donor

AAA**ATG**GCTGAACATTTTTTGTACAGAAGAAGCGTCCAACGAGAGCAAACGCCGTGAGACCGTG
TGTTTTCGCAGCGAATTACGCCAATAAAACCGCACTAAGAGCGCGCTCGCAGCGCGAATAAAGA
ATAGCAGCCGCGTATGGACGAAATGCGGCACGAATCGCTGGAAAAATCGACGGCCAGACCGAAA
AATAGCAGCGAAATTCGAGCGAACGTCGTGTATAAGTAAAACGAAAGTTGTGTCGCTCTGTGCG
AAAGAGAGAGGGAGAACCCAATATTTTTGCAAGCCAGAAGTCGAAGGTGAAATTAAAATGCATT
AGCCACCCAATTGAAGAGGAGTCAACTACGAACAAAACTTTAAGAATCAGCGAAAAATCGTTTG
TGAACATCCATACAAGCACAAATCGTTGTTTTTGCCTGCTCTCGTGTAGTTCCTGTGTATTGGT
GCGCGCGCCCTGTGTGTGTTTGTGCGTGTGCGTGCGTGTAAGCATTGGAATGGATTAACTACCC
AACTAATTCCAAAACAATAATACCGCAACATAATCGCAATAGTCATGCCGTTTCAAGGCGACAG
CCTTTAGGGAAACATTCGGTCGGTCGGTCAGTCAACCAAAAATCAGTTGCTATAATTAGCACGC
CCACGTTTTAATTTCAACGATCGCCAGCAACCGCCTACGCGGTTAAATCGCAGGACTTCGCCAA
CATGGATATGGATTTGGAGCAGCTAAAGAACGACTTCCTGCCGCTTATCGCCGGGATCAAGCAG
GAGCAGCTGGATGCCGTGCCCACGGATGCCCTGCCCCAGATGAGCACACCAAACACGGCCAGCG
GTGCGCCCACAACCTCGTCATTGAGCTCCTCTTCGCTGAGTCTGAGCAACCCCTGCGACAGTGC
CGAGAAAAG

B. translated

⮟ *bonus*^{21B} deleted from +12 to past exon 1 splice donor

K **M** A E H F L Y R R S V Q R E Q T P * D R V F S Q R I T P I K P
H * E R A R S A N K E * Q P R M D E M R H E S L E K S T A R P K
N S S E I R A N V V Y K * N E S C V A L C E R E R E N P I F L Q
A R S R R * N * N A L A T Q L K R S Q L R T K L * E S A K N R L
* T S I Q A Q I V V F A C S R V V P V Y W C A R P V C V C A C A
C V * A L E W I N Y P T N S K T I I P Q H N R N S H A V S R R Q
P L G K H S V G R S V N Q K S V A I I S T P T F * F Q R S P A T
A Y A V K S Q D F A N M D M D L E Q L K N D F L P L I A G I K Q
E Q L D A V P T D A L P Q M S T P N T A S G A P T T S S L S S S
S L S L S N P C D S A E K

Fig. S10. Cryptic methionine in *bonus*^{21B} may yield a nearly full-length protein. A) Complete DNA sequence of *bonus* exon1 indicating the start of the deletion in *bonus*^{21B} and the presence of a start codon (bold) in the remaining transcribed sequence. Sequences encoding the Bonus open reading frame are in red. B) Translation of *bonus* exon1 revealing the cryptic Methionine (bold) and the 66 amino acids of the Bonus protein (red) that would be missing if the cryptic Methionine were able to splice into exon2 in frame. Previously Table S2 showed that the Ring domain of Bonus begins at amino acid 83 and thus none of the defined domains are located in the deleted region of exon1.

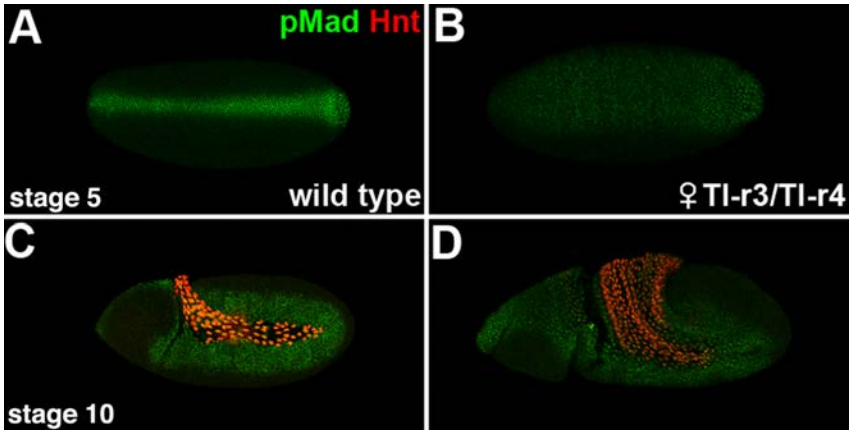

Fig. S11. Reduction in maternal Toll signaling leads to expanded pMad and Hindsight expression. A) Stage 5 wild type embryo in dorsal view displaying a sharp dorsal nuclear stripe of pMad expression. B) Stage 5 embryo in dorsal view from a $Toll^{r3}/Toll^{r4}$ female mated to a wild type male. The reduction in maternal Toll signaling associated with these loss of function alleles is reflected in a broad, ventrally expanded pMad stripe. C) Stage 10 wild type embryo in lateral view displaying Hindsight in the amnioserosa and a wide, lateral ectoderm stripe of pMad. D) Stage 10 embryo in lateral view from a $Toll^{r3}/Toll^{r4}$ female mated to a wild type male. The reduction in maternal Toll signaling is reflected in the ventral expansion of both Hindsight and pMad.

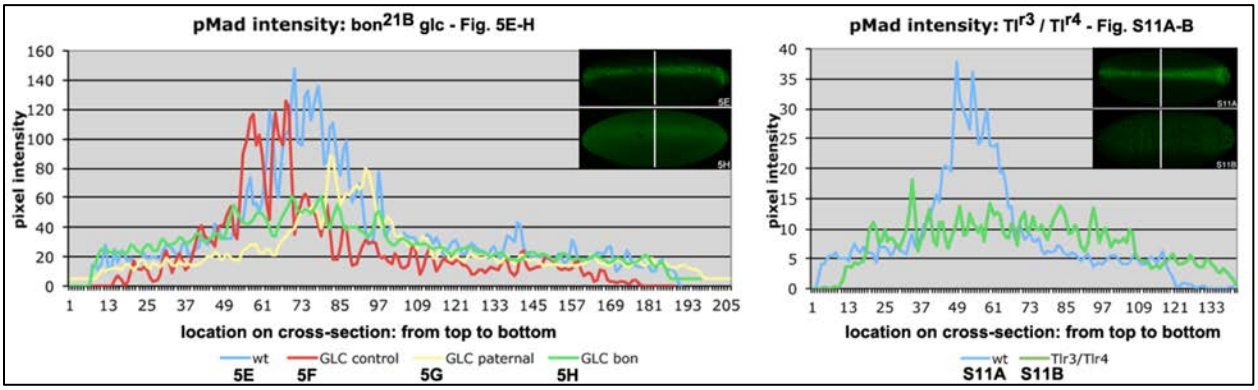

Fig. S12. *Bonus*^{21B} germline clone and maternal *Toll*^{r3}/*Toll*^{r4} similarly effect pMad expression. Pixel intensities along a cross section from top to bottom on each image are shown from left to right in each graph employing arbitrary units. Left: Intensities for the green (pMad) channel from each of the four genotypes shown in Fig. 5E-H are graphed. The wild type and *bonus*^{21B} germline clone embryos with the location of their cross section lines are shown as insets. The legend indicates the color associated with each genotype. Right: Intensities for the green (pMad) channel from the two genotypes shown in Fig. S11A,B are graphed. The wild type and maternal *Toll*^{r3}/*Toll*^{r4} embryos with the location of their cross section lines are shown as insets. Note that in both graphs the blue peak (wild type) is considerably narrower and sharper than the green peak (*bonus*^{21B} germline clones or maternal *Toll*^{r3}/*Toll*^{r4}).

NP_724052.1 Dorsal, isoform A [Drosophila melanogaster]

MFPNQNNGAAPGQGPAVDGQQSLNYNGLPAQQQQQLAQSTKNVRKKPYVKITEQPAGKALRFRY
ECEGRSAGSIPGVNSTPENKTYPTIEIVGYKGRAVVVVSCVTKDTPYRPHPHNLVGKEGCKKGV
CTLEINSETMRAVFSNLGIQCVKKKDIEAALKAREEIRVDPFKTGFSHRFQPSSIDLNSVRLCF
QVFMESEQKGRFTSPLPPVVSEPIFDKKAMSDLVICRLCSCSATVFGNTQIILLCEKVAKEDIS
VRFFEEKNGQSVWEAFGDFQHTDVHKQTAITFKTPRYHTLDITEPAKVFIQLRRPSDGVTSEAL
PFEYVPMDSDPAHLRRKRQKTGGDPMHLLLQQQQKQQLQNDHQDGRQTNMNCWNTQNIPPIKTE
PRDTSPQPFGLSYRAPPELTPSPQPLSPSSNYNHNSTPSPYNMASAVTPTNGQQQLMSPNHPQQ
QQQQQQYGATDLGSNYNPFAQQVLAQQQQHQQQQQQHQHQHQQQHQQQQQQQQQQQQQSLQFHA
NPFGNPGGNSWESKFSAAAVAAAAATATGAAPANGNSNNLSNLNNPFTMHNLLTSGGGPGNANN
LQWNLTTNHLHNQHTLHQQQQLQQQQQQQYDNTAPTNNNANLNNNNNNNNTAGNQADNNGPTLS
NLLSFDSGQLVHINSEDQQILRLNSEDLQISNLSIST

Fig. S13. Dorsal contains a candidate Bonus-interacting AF-2 AD domain. Bonus physically interacts with the AF-2 AD domain in βFTz-F1 (Beckstead et al., 2001). This domain has the consensus hhXEhh (h = hydrophobic amino acid, X = any amino acid, E = glutamic acid). Dorsal (red residues 211-216) contains a near-perfect match to this consensus with a weakly hydrophobic proline in the penultimate position.

Beckstead R, Ortiz J, Sanchez C, Prokopenko S, Chambon P, Losson R, Bellen HJ. 2001. Bonus, a *Drosophila* homolog of TIF1 proteins, interacts with nuclear receptors and can inhibit FTZ-F1-dependent transcription. *Mol Cell* 7:753-765.

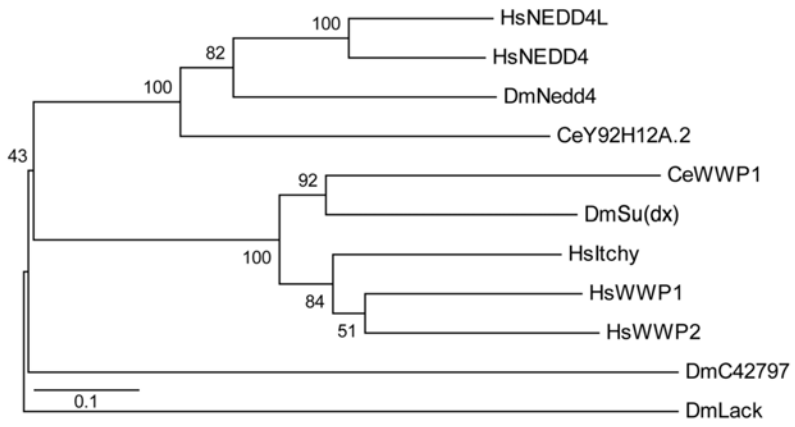

Fig. S14. Maximum likelihood tree of fly Nedd4 and closely related proteins. An unrooted tree generated from an alignment of the eleven sequences from human (Hs), fly (Dm) and nematode (Ce) most closely related to *Drosophila* Nedd4. These are all C2 and WW domain containing HECT class E-3 ubiquitin ligases (Grau-Bové et al., 2013). The statistically supported Nedd4 cluster contains a single member in flies and nematodes with two in humans.

Accession numbers (we employed the longest isoform as noted):

CeWWP1-NP_740775 (isoformA)

CeY92H12A.2-NP_490865

DmC42797-NP_001188572 (isoformE)

DmLack/dSmurf-NP_523779 (isoformA)

DmNedd4-NP_648993 (isoformJ)

DmSu(dx)-NP_722753 (isoformA)

HsItchy-NP_001244066 (isoform1)

HsNEDD4-NP_006145 (isoform1)

HsNEDD4L-NP_001138439 (isoform1)

HsWWP1-NP_008944

HsWWP2-NP_001257383 (isoformFL)

Grau-Bové X, Sebé-Pedrós A, Ruiz-Trillo I. 2013. A genomic survey of HECT ubiquitin ligases in eukaryotes reveals independent expansions of the HECT system in several lineages. *Genome Biol Evol*. 5:833-847.